A TWO-STEP COMPUTATIONAL HOMOGENIZATION APPROACH FOR DETERMINATION OF ELASTIC CONSTANTS OF HYBRID COMPOSITES

A THESIS SUBMITTED TO
THE GRADUATE SCHOOL OF NATURAL AND APPLIED SCIENCES
OF
MIDDLE EAST TECHNICAL UNIVERSITY

BY

MUSA BATIR

IN PARTIAL FULFILLMENT OF THE REQUIREMENTS
FOR
THE DEGREE OF MASTER OF SCIENCE
IN
AEROSPACE ENGINEERING

SEPTEMBER 2023

Approval of the thesis:

A TWO-STEP COMPUTATIONAL HOMOGENIZATION APPROACH FOR DETERMINATION OF ELASTIC CONSTANTS OF HYBRID COMPOSITES

submitted by **MUSA BATIR** in partial fulfillment of the requirements for the degree of **Master of Science in Aerospace Engineering Department, Middle East Technical University** by,

Prof. Dr. Halil Kalıpçılar
Dean, Graduate School of **Natural and Applied Sciences** _____

Prof. Dr. Serkan Özgen
Head of Department, **Aerospace Engineering** _____

Assoc. Prof. Dr. Ercan Gürses
Supervisor, **Aerospace Engineering, METU** _____

Examining Committee Members:

Prof. Dr. Demirkan Çöker
Aerospace Engineering, METU _____

Assoc. Prof. Dr. Ercan Gürses
Aerospace Engineering, METU _____

Assist. Prof. Dr. Görkem Eğemen Güloğlu
Aerospace Engineering, METU _____

Assoc. Prof. Dr. Serdar Göktepe
Civil Engineering, METU _____

Assoc. Prof. Dr. Barış Sabuncuoğlu
Mechanical Engineering, Hacettepe University _____

Date:08.09.2023

I hereby declare that all information in this document has been obtained and presented in accordance with academic rules and ethical conduct. I also declare that, as required by these rules and conduct, I have fully cited and referenced all material and results that are not original to this work.

Name, Surname: Musa Batır

Signature :

ABSTRACT

A TWO-STEP COMPUTATIONAL HOMOGENIZATION APPROACH FOR DETERMINATION OF ELASTIC CONSTANTS OF HYBRID COMPOSITES

Batır, Musa
M.S., Department of Aerospace Engineering
Supervisor: Assoc. Prof. Dr. Ercan Gürses

September 2023, 77 pages

Carbon-fiber-reinforced polymer composites consist of carbon as a reinforcement element and polymer as a matrix. This kind of material shows unique mechanical properties. Because of the deficiency of adhesion properties, transverse mechanical properties are not as good as longitudinal properties. This restricts the use of carbon-reinforced polymer composites. Carbon Nanotubes can be grown on the surface of carbon fiber as an interphase to increase the transverse properties of the material. This material is called fuzzy fiber composites (FFC) or hybrid composites. Both the manufacturing and the characterization of the produced material are very challenging.

The study's main aim is to characterize the fuzzy fiber composite with the help of homogenization techniques. By using micromechanical and numerical methods, a new two-step homogenization method is proposed to calculate the effective mechanical properties of this hybrid composite. At first, a micromechanical method, i.e., Mori-Tanaka, is followed to obtain the mechanical properties of the graded interphase region. FEM analyses are conducted for a representative volume element (RVE) after determining the interphase's homogenized properties.

This study conducts several parametric studies using the proposed two-step homog-

enization approach. The effects of CNT length, CNT volume fraction, and fiber volume fraction are investigated. Parametric studies are performed via engineering material constants. Engineering material constants are calculated from the effective elasticity tensor of the constitutive model obtained by the two-step homogenization approach.

Keywords: homogenization, interphase, hybrid composites, fuzzy fiber composites, carbon nanotubes, finite element method, effective modulus, micromechanics

ÖZ

İKİ BASAMAKLI HESAPLAMALI HOMOJENLEŞTİRME YAKLAŞIMI KULLANARAK HİBRİT KOMPOZİTLERİN ELASTİK SABİTLERİNİN SAPTANMASI

Batır, Musa
Yüksek Lisans, Havacılık ve Uzay Mühendisliği Bölümü
Tez Yöneticisi: Doç. Dr. Ercan Gürses

Eylül 2023 , 77 sayfa

Karbon fiber takviyeli polimer kompozitler, takviye elemanı olarak karbondan ve matris olarak polimerden oluşur. Bu tür malzemeler benzersiz mekanik özellikler gösterir. Adezyon özelliklerinin yetersizliğinden dolayı, transvers mekanik özellikler eksenel özellikler kadar iyi değildir. Bu durum karbon takviyeli polimer kompozitlerin kullanım alanını kısıtlamaktadır. Karbon Nanotüpler (KNT), malzemenin transvers özelliklerini artırmak için bir arafaz olarak karbon fiberin yüzeyinde büyütülebilir. Bu malzemeye bulanık (fuzzy) fiber kompozit (BFK) veya hibrit kompozit denilmektedir. Üretilen malzemenin hem üretimi hem de karakterizasyonu çok zordur.

Çalışmanın temel amacı, bulanık fiber kompoziti homojenleştirme teknikleri yardımıyla karakterize etmektir. Mikromekanik ve hesaplamalı yöntemlerle, bu hibrit kompozitin efektif mekanik özelliklerini hesaplamak için iki aşamalı yeni bir homojenleştirme yöntemi önerilmektedir. Kademeli interfaz bölgesinin mekanik özelliklerini elde etmek için ilk önce mikromekanik bir yöntem izlenmektedir. Ara fazın homojenleştirilmiş özellikleri elde edildikten sonra temsili bir hacim elemanının sonlu ele-

menlar yöntemi yardımıyla analizleri gerçekleştirilmektedir.
Bu çalışma, önerilen iki aşamalı homojenleştirme yaklaşımını kullanarak birkaç parametrik çalışma yürütmektedir. KNT uzunluğunun, KNT hacim fraksiyonunun ve fiber hacim fraksiyonunun etkisi araştırılmaktadır. Parametrik çalışmalar mühendislik malzeme sabitleri üzerinden yapılmaktadır. Mühendislik malzemesi sabitleri, iki aşamalı homojenleştirme yaklaşımıyla elde edilen konstitütif modelin etkin esneklik tensöründen hesaplanmaktadır.

Anahtar Kelimeler: homojenleştirme, arafaz, hibrit kompozitler, bulanık fiber kompozitler, karbon nanotüp, sonlu elemanlar yöntemi, efektif modül, mikromekanik

To my mom, Şekernaz Batır

ACKNOWLEDGMENTS

First and foremost, I would like to express my deepest gratitude to my advisor, Assoc. Prof. Dr. Ercan Gürses for his endless encouragement, guidance, criticism, and insight from the very first day of graduate education and the very first page of this thesis until the last day and word of it.

I would like to thank to the thesis committee members, Prof. Dr. Demirkan Çöker, Assoc. Prof. Dr. Serdar Göktepe, Assoc. Prof. Dr. Barış Sabuncuoğlu, and Asst. Prof. Dr. Görkem Eğemen Güloğlu for their valuable participation, interest, and contribution to the thesis.

I would like to thank my parents, Hüseyin and Şekernaz Batır, sister, Şahsenem Korkmaz, and brothers, Adem and Erdem Batır, for their endless love and support.

I would like to thank to my friends Gizem Yıldırım, Deniz Çevik, Barış Öztaş, Huzeyfe Kocabaş, and Abdullah Berküz for their encouragement, friendship, and support.

Finally, I would like to give my deepest thanks to my friend and classmate Alperen Demirtaş, with whom I worked for the Tübitak project, for his help and contributions to the thesis, support, and joyfulness.

TABLE OF CONTENTS

ABSTRACT v

ÖZ vii

ACKNOWLEDGMENTS x

TABLE OF CONTENTS xi

LIST OF TABLES xiv

LIST OF FIGURES xvi

LIST OF ABBREVIATIONS xix

CHAPTERS

1 INTRODUCTION 1

1.1 Motivation and Aim of Thesis 2

1.2 Outline and Scope of Thesis 3

2 FUZZY FIBER COMPOSITES 5

2.1 Characterization of FFC 7

2.2 Manufacturing of FFC 9

3 HOMOGENIZATION 11

3.1 Analytical methods 12

3.2 Computational methods 17

3.2.1 Linear Displacement Boundary Condition 19

3.2.2 Periodic Boundary Condition 19

3.2.3 Uniform Traction Boundary Condition 20

4 METHODOLOGY 21

4.1 Computational Homogenization Approach 22

4.2 Homogenization of the Interphase 27

4.3 Homogenization of the FFC 31

5 RESULTS 37

5.1 Comparison with Literature 39

5.1.1 Comparison with Micromechanical and Computational Approaches 40

5.1.2 Comparison with Experimental Study 42

5.2 Effects of the CNT Volume Fraction 44

5.3 Effects of the CNT Length 47

5.4 Effects of the Fiber Volume Fraction 49

6 CONCLUSION 53

REFERENCES 57

A 63

A.1 Inverse of a Symmetric Fourth-Order Tensor 63

B 65

B.1 Comparative Study of Periodic Boundary Conditions and Linear Displacement Boundary Conditions 65

C 69

C.1 FORTRAN Script for the Homogenization of Interphase 69

D 71

D.1 MATLAB Script for the Homogenization of FFC 71

LIST OF TABLES

TABLES

Table 3.1 Material properties of homogenization examples. 13

Table 4.1 The engineering material properties of carbon fiber, CNT, and epoxy. 21

Table 4.2 Load cases applied with linear displacement boundary condition to the RVE consisting of single CNT and epoxy matrix. 28

Table 4.3 Comparison of Mori-Tanaka and FE results for the interphase region. 30

Table 5.1 The parameters used in the comparison with the literature study with the fiber radius of 5 micrometers. 40

Table 5.2 Transverse elastic modulus obtained from experimental study [1] and [2]. 42

Table 5.3 The engineering material properties of carbon fiber, CNT, and epoxy for the study of comparison with literature. 43

Table 5.4 Transverse elastic moduli of FFCs with CNT volume fraction of 2% and FRP obtained from the two-step computational homogenization approach. 43

Table 5.5 The fixed parameters in the effects of the CNT volume fraction study with the fiber radius of 5 micrometers. 44

Table 5.6 CNT numbers corresponding to CNT volume fraction in the study of the effect of the CNT volume fraction for the varying CNT number case. 45

Table 5.7 CNT lengths corresponding to CNT volume fraction in the study of the effect of the CNT volume fraction for the varying CNT length case. . . 45

Table 5.8 The parameters in the effects of the CNT length study with the constant CNT volume fraction. 48

Table 5.9 The parameters in the effects of the fiber volume fraction study with the constant CNT volume fraction. 49

Table B.1 Comparison of DBC and PBC results for different aspect ratios of the RVE. 66

LIST OF FIGURES

FIGURES

Figure 1.1 Introduction of interphase [3]. 2

Figure 2.1 Rooling a graphene sheet into CNT [4]. 5

Figure 2.2 Representation of a single-walled CNT and multi-walled CNT [5]. 6

Figure 2.3 Representation of FFC where fiber is colored purple, CNTs are colored black, and the matrix is colored green. 7

Figure 2.4 SEM image of carbon fiber coated with CNTs [6]. 8

Figure 2.5 Experimental setup representation: (a) DCD test, (b) ENF test [7]. 10

Figure 3.1 Concept of heterogeneous (left) and homogenized (right) media. 11

Figure 3.2 Voigt and Reuss bound comparison example. 13

Figure 3.3 Hashin-Shtrikman bounds comparison example. 14

Figure 3.4 Comparison of different analytical homogenization approaches. . 17

Figure 3.5 Discritization of a RVE for PBC [8]. 20

Figure 4.1 Engineering constants of a transversely isotropic material [9]. . . 27

Figure 4.2 FE model of RVE of CNT for the aspect ratio of CNT of 2. . . . 27

Figure 4.3 Representation of FFC: (a) 3D RVE of FFC; (b) CNTs on fiber surface from top view; (c) RVE of a single CNT; (d) Reduction in CNT volume fraction representation [10]. 29

Figure 4.4 FE model of the FFC. 31

Figure 4.5 Defining datum coordinate systems to the fiber (a) and the interphase (b) in ABAQUS. 32

Figure 4.6 Linear displacement boundary conditions in ABAQUS. (a) Normal loading in the fiber direction. (b) Normal loading in the transverse direction. (c) Simple shear loading parallel to the fiber direction. 34

Figure 4.7 Schematic procedures of the two-step computational homogenization of the FFC. 35

Figure 5.1 Variation of local volume fraction of CNTs in interphase as a function of distance from the fiber surface. 37

Figure 5.2 Effective interphase properties for total CNT volume fraction of 7% and fiber radius of 5 micrometers. 38

Figure 5.3 Illustration of undeformed and deformed shapes of the cubic RVE. (a) Undeformed RVE. (b) Normal loading in the fiber direction. (c) Normal loading in the transverse direction. (d) Simple shear loading parallel to the fiber direction. 39

Figure 5.4 Comparison of the results obtained by two-step homogenization approach and Cheng et al. [9] (hierarchical homogenization- MM and FEM). 41

Figure 5.5 Illustrations of 2D RVE consisting of single CNT and a matrix. (a) A CNT volume fraction is less than the maximum value. (b) The maximum volume fraction of CNT where the CNT touches the boundary of the RVE. 45

Figure 5.6 : Effects of the CNT volume fraction on engineering constants. The length of the CNTs is 2 micrometers for the varying CNT number case. 46

Figure 5.7 Effects of the CNT length on engineering constants. The CNT volume fraction is constant and 9.42% in the study. The fiber radius is 5 micrometers, and the fiber volume fraction is 20%. 48

Figure 5.8 Effects of the fiber volume fraction on engineering constants. The CNT volume fraction is constant and 9.42% in the study; the length (2 micrometers) and the number (8×10^6) of CNTs are fixed, which results in different local CNT volume fractions in the interphase regions. 50

Figure B.1 The RVE of the simple model consists of 2 constituents, and the fiber is a square prism. 65

Figure B.2 Illustrations of applications of (a) PBCs and (b) DBCs. 66

Figure B.3 Comparison of DBC and PBC results for different aspect ratios of the RVE. 67

LIST OF ABBREVIATIONS

ASTM	American Society for Testing Materials
BC	Boundary Condition
CNT	Carbon Nanotube
CCVD	Catalyst Chemical Vapor Deposition
CVD	Chemical Vapor Deposition
DBC	Linear Displacement Boundary Condition
DCB	Double Cantilever Beam
ENF	End-notch Flexure
EPD	Electrophoretic Deposition
FE	Finite Element
FEM	Finite Element Method
FFC	Fuzzy Finer Composite
MOC	Method of Cell
PBC	Periodic Boundary Condition
RVE	Representative Volume Element
TBC	Uniform Traction Boundary Condition

CHAPTER 1

INTRODUCTION

A composite material is a material that consists of at least two different constituents, generally an inclusion and a matrix. With this constitution, it becomes very functional due to its superior properties, such as lightweight, higher strength, high impact resistance, and resistance to fatigue and corrosion. Moreover, composite materials can be tailored according to where they will be used, giving them a considerable utilization area. Thus, they are widely used in many sectors, such as aerospace, civil, medical engineering, etc. Since the discovery of carbon fibers, carbon-reinforced polymer composites, which consist of carbon as an inclusion and a polymer matrix, have gained importance for their structural performance. However, despite these materials' successful structural performance, the fiber-matrix interface's poor mechanical properties restrict the composites' novel properties. To enhance the mechanical properties of the interface between the fiber and matrix, the most common technique is introducing a third phase between the fiber and matrix, named interphase, as shown in Figure 1.1 [11]. As interphase, carbon nanotubes can improve the interfacial adhesion properties and increase the fiber's surface area [12].

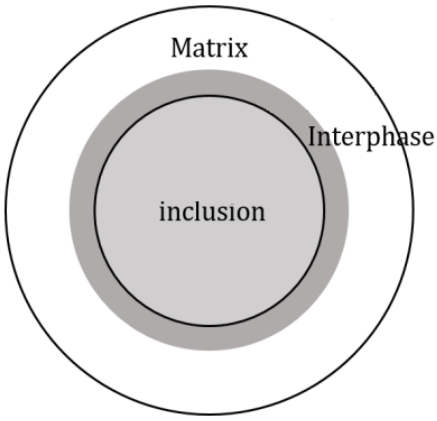


Figure 1.1: Introduction of interphase [3].

1.1 Motivation and Aim of Thesis

Advanced composites have many challenging problems, such as preparation, synthesis, processing, and characterization. The study focuses on the characterization of hybrid composites with the help of the computational homogenization method. Characterization of hybrid composites is a challenging process. Hybrid composites have at least three constituents, making their homogenization procedure more complex. To characterize the hybrid composites, a new homogenization method is proposed. A two-step homogenization approach will be followed to understand the overall macroscopic behavior of the composite. Two steps are needed because of the complex structure of the interphase region. The interphase region has a mechanically graded property because of radially aligned CNTs. Therefore, in the first step, the interphase region will be homogenized. After obtaining the homogenized properties of the interphase, the overall macroscopic behavior of the hybrid composite will be determined by the homogenization procedure as a second step. Selection and the application of the appropriate homogenization and characterization methods play vital roles. For this purpose, analytical and three-dimensional finite element codes are developed and combined in two steps to characterize the overall properties of the hybrid composites.

1.2 Outline and Scope of Thesis

In Chapter 2, the definition and the structure of fuzzy fiber composites (FFCs) and carbon nanotubes are given. Related studies from the literature are mentioned briefly. The advantages of CNT grafting and the mechanical and electrical property enhancements from the related studies are discussed in the characterization sub-section. Manufacturing of the FFC, as the other challenging side of the area, is concerned, and different manufacturing methods are compared.

In Chapter 3, the concept of homogenization is explained. Mainly, analytical homogenization methods are discussed and compared with each other. Voigt-Reuss and the Hashin-Shtrikman bounds are presented. The Mori-Tanaka method is compared with these bounds. Besides the analytical methods, computational methods are briefly explained. The engineering constants are obtained through the Voigt notation, and definitions of engineering constants are presented.

In Chapter 4, the proposed methodology to homogenize the FFC is explained in a detailed way. The Mori-Tanaka method is preferred for the homogenization of the interphase, and implementation of the method to a finite element solver is given. The graded structure of the interphase is discussed, and the implementation of the graded properties of the region in the proposed method is demonstrated. The selection of the appropriate boundary condition for the representative volume element of the hybrid composite is explained with a comparative study. A two-step computational homogenization scheme is constructed and presented.

In Chapter 5, homogenized engineering properties of the FFC obtained by the two-step computational homogenization method are given. Parametric studies of fiber volume fraction, CNT volume fraction, and CNT length are presented and discussed. The effects of CNT growth on fiber is discussed.

Chapter 6 summarizes the thesis and presents conclusions and suggestions for future work.

CHAPTER 2

FUZZY FIBER COMPOSITES

Carbon nanotubes (CNT) were discovered by Sumio Iijima, a Japanese scientist, in 1991. Since their discovery, nanoscience has become the focus of much scientific research because of the possibility of using the CNTs in smaller systems that can be on the nanoscale. As the name implies, CNT is one of the allotropes of carbon, which has a hexagonal package of carbon atoms rolled into a tubular shape. The nanotube's name comes from the tube's diameter in nanosize. The tube length is in the micro size, which makes the aspect ratio (size ratio length to diameter) of the CNTs in the order of thousands. Syntheses of CNTs are achieved by rolling the graphene sheet into a tubular shape. In the literature, it is stated that CNTs are produced by three techniques. These are chemical vapor deposition, arc discharge, and laser ablation [13].

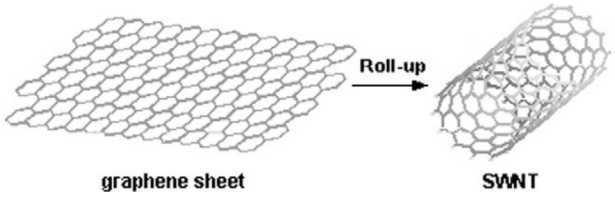


Figure 2.1: Rooling a graphene sheet into CNT [4].

Types of CNTs are considered under two main categories: single-walled carbon nanotubes (SWCNT) and multi-walled carbon nanotubes (MWCNT). SWCNTs are formed by rolling just one graphene sheet into a tube, as seen in Figure 2.1. MWCNTs are formed with multiple layers of graphene sheets, which can be considered

the collection of concentric SWCNTs with different diameters, as illustrated in Figure 2.2. Despite the SWCNT's excellent electric properties, MWCNTs are not good conductors because of the space between the walls.

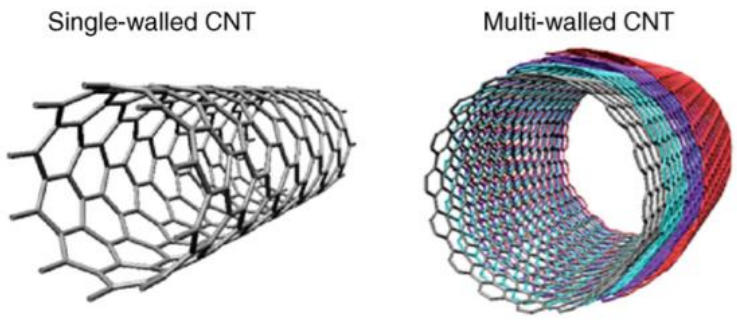


Figure 2.2: Representation of a single-walled CNT and multi-walled CNT [5].

In recent years, hybrid composites have gained importance with the discovery of CNT's superior mechanical and electrical properties and strong interaction between CNT and polymer [14]. The addition of CNTs in any polymer matrix composites is applicable due to their nanoscale size and provides promising enhancements to the mechanical and electrical properties of the composite system. A fuzzy fiber composite (FFC) is a material that the inclusion is carbon fiber. Around the fiber, there are radially grown CNTs (forests of carbon nanotubes) on the fiber, as schematically shown in Figure 2.3. A scanning electron microscope (SEM) image of a fuzzy fiber is shown in Figure 2.4. Because of the interphase's bristled structure, these materials are called fuzzy fiber composites. In the literature, plenty of experiments have already validated the properties of FFCs, such as flexural elastic modulus, inter-laminar shear strength, and fracture toughness.

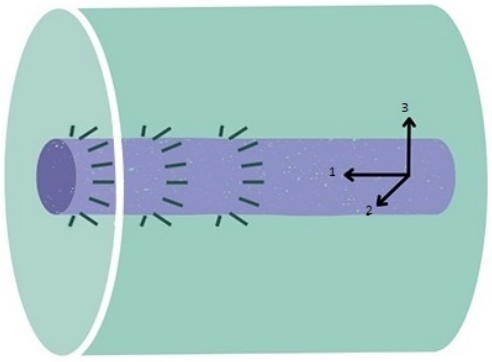


Figure 2.3: Representation of FFC where fiber is colored purple, CNTs are colored black, and the matrix is colored green.

2.1 Characterization of FFC

In the study of Cheng et al. [9], FFC is compared with traditional fiber-reinforced composites. FFC is characterized through the hierarchical model using the micromechanics-based Mori-Tanaka method. The hierarchical model is proposed because of the graded structure of the CNT grafted interphase region caused by the variation of the local volume fraction of the CNT in the interphase region. At first, the Mori-Tanaka method is used to homogenize the CNT region, and then a multi-coated model is obtained. After that, in the meso scale, sequential homogenization steps are performed to obtain the effective properties of the macro scale composite. This study showed that the transverse modulus increases by 30% - 50%, and the shear modulus increases by more than 20%. The tensile modulus is almost unaffected; the change in tensile modulus is less than 1.5%.

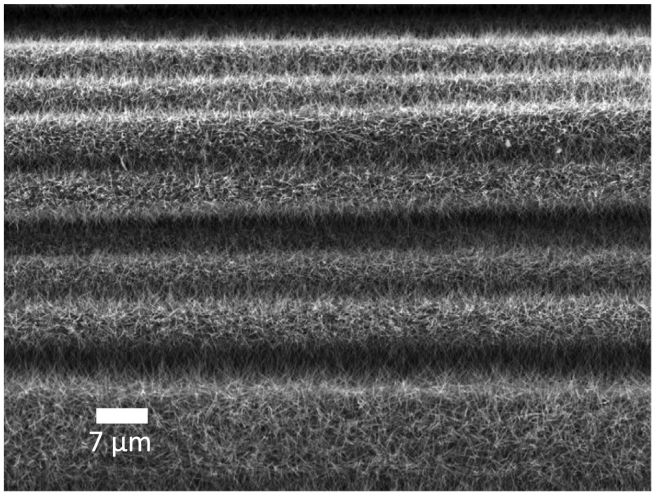


Figure 2.4: SEM image of carbon fiber coated with CNTs [6].

Wicks et al. [15] studied the experimental characterization of fuzzy fiber composites. Fuzzy fiber plies are fabricated for the tests. Following the American Society for Testing Materials (ASTM) standards, short-beam, tension-bearing, and single-shear-bearing tests are conducted. According to the results of the tension-bearing testing, fuzzy fiber plies show enhanced properties in the chord stiffness, offset bearing strength, and ultimate bearing strength. The interlaminar shear strength of the FFC increased by approximately 70% compared to the baseline composite by the results of the short-beam shear test. Similar results for the interlaminar shear strength are obtained from the short beam test, which Garcia et al. [16] conducted regarding ASTM. The tests proved that the composites' interlaminar and intralaminar mechanical properties are enhanced.

Wood et al. [17] studied hybrid glass fibers. Multi-walled carbon nanotubes are grafted on the surface of the glass fibers by chemical vapor deposition. The study presents a new technique for characterizing the hybrid composite. They showed an approximately 35% enhancement in the stiffness values of the composite. This study shows that the grafting CNTs on a fiber, whether carbon or not, increases the mechanical properties of the composite.

Grafting CNT on the fiber increases not only the mechanical properties but also the electrical properties of the composite system. Dhala and Ray [18] studied the electri-

cal effective properties of CNT-grafted piezoelectric fibers. The composite is modeled by the method of cell and Mori-Tanaka method. The results show that piezoelectric constants e_{31} and e_{32} are significantly larger than their values without CNTs. Radially grown CNTs cause in-plane stiffening (parallel to the fiber axis), which enhances the composite's piezoelectric behavior. Also, De Luca et al. [19] showed that the presence of the CNTs increases the electrical conductivity of the composite beyond the initial value.

2.2 Manufacturing of FFC

Manufacturing FFC is a challenging process compared to traditional composite materials. If the CNT is not grown with unique techniques, mechanical properties become very poor. It decreases beyond the properties of conventional carbon fiber composites. Shan et al. [7] introduced a new technique to significantly improve carbon-reinforced polymers' out-of-plane properties. A new spraying technique is E20 for coating carbon surfaces with CNT. Also, chemical vapor deposition (CVD) is used to manufacture this material. In the study of Shan et al. [7], differently treated carbon fiber fabrics are manufactured and tested. A comparative study was performed between these composites: as-received fabric, CNT-grafted fabric with the E20 spraying technique, and CNT-grafted fabri without the E20 spraying technique. For the experimental setup, double cantilever beam (DCB) and end-notch flexure (ENF) tests are conducted according to ASTM. The representation of experimental setups is illustrated in Figure 2.5. The results showed that the mechanical properties of the CNT-grafted fabric with the E20 spraying technique are increased by between 10% and 25% compared to the as-received fabric. However, the mechanical properties of the CNT-grafted fabric without E20 are decreased by around 10% beyond the as-received fabric properties.

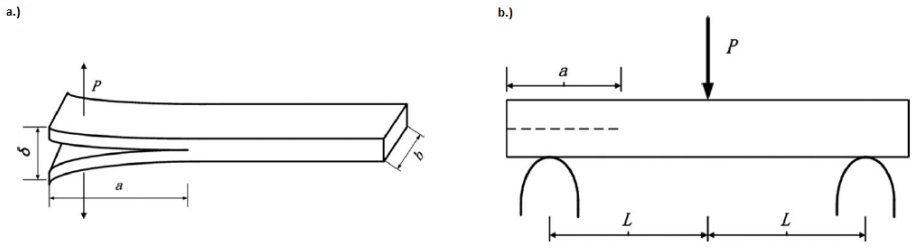


Figure 2.5: Experimental setup representation: (a) DCD test, (b) ENF test [7].

Li et al. [20] compared the two manufacturing methods of the FFC; catalyst chemical vapor deposition (CCVD) and Electrophoretic deposition (EPD). It is stated in the study that CCVD has the disadvantages of high cost and process complexity. In the CCVD method, harsh chemical treatments can damage the carbon fibers' surface. EPD is a low-cost and simple method as an alternative to CCVD. EPD manufacturing method offers control of deposit thickness, microstructural homogeneity, and uniformity of deposits. EPD helps to avoid the damaged surface structure of the carbon fiber in the absence of harsh chemical treatments.

CHAPTER 3

HOMOGENIZATION

In nature, almost every material exhibits some level of heterogeneity. In a heterogeneous medium, the properties, which can be mechanical, electrical, or thermal, change in the continuous medium. Therefore, understanding the behavior of a heterogeneous material on a macroscopic scale becomes very important. The homogenization theory can calculate the material's behavior on a macroscopic scale, as illustrated in Figure 3.1. With the help of homogenization theory, the heterogeneous material's effective properties can be obtained. In this perspective, every composite material consisting of at least two constituents is considered heterogeneous. Homogenization theory can be used to obtain the effective mechanical properties of the composite material.

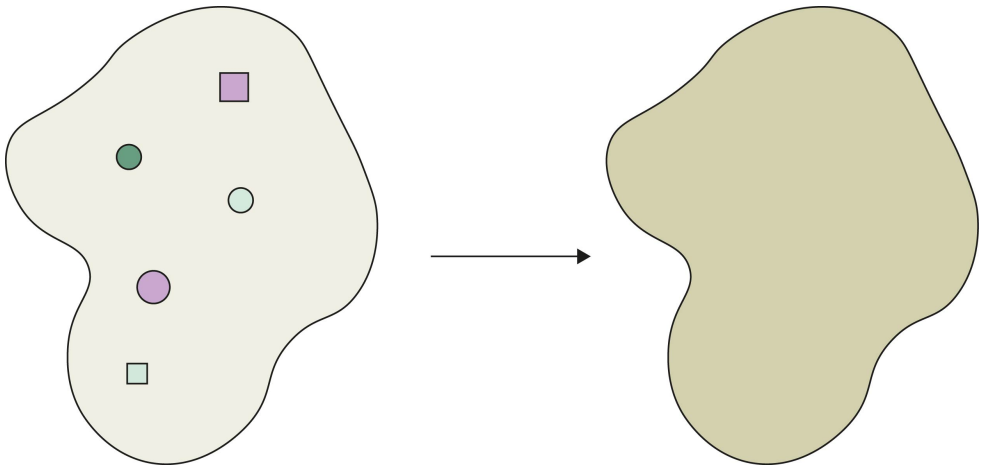


Figure 3.1: Concept of heterogeneous (left) and homogenized (right) media.

In 1963, Hill [21] introduced the concept of representative volume element (RVE),

which provides a huge utilization area for composite materials. A representative volume element is a finite-sized sample of the composite material as an example of a heterogeneous material, which characterizes the macroscopic behavior of the heterogeneous material. Results obtained from the RVE can be attributed to the overall material. Instead of analyzing a large material, this finite-sized sample ensures an easy way for the homogenization theory. Testing the RVE with appropriate boundary conditions is very important to utilize the homogenization method. One of the three boundary conditions, linear displacement, periodic, or uniform traction boundary conditions, is commonly employed depending on the problem.

3.1 Analytical methods

The Voight and Reuss methods [22], [23], the so-called upper and lower bounds, are the most known methods for heterogeneous material. These methods are also known as the rule of mixture and the inverse rule of mixture. Because of the assumptions of constant stress and strain fields, these methods give the upper and lower bounds for the macroscopic elasticity tensor. It is expected that the material behavior should be within these bounds. For the Voigt bound, which assumes a constant strain over the domain, and the Reus bound, which assumes a constant stress over the domain, the calculation of any elastic property of the material relies on the volume fraction of the constituents. For simplicity, a two-phase formulation of the Voigt bound is considered. Also, there are other methods to calculate the effective properties of heterogeneous material, such as the Hashin-Shtrikman approach and the Hill average method.

$$D_{Voigt} = \nu_1 D_1 + \nu_2 D_2 \tag{3.1}$$

$$\frac{1}{D_{Reuss}} = \frac{\nu_1}{D_1} + \frac{\nu_2}{D_2}, \tag{3.2}$$

where D_1 and ν_1 are any elastic property and volume fraction ratio of phase 1. D_2 and ν_2 are any elastic property and volume fraction ratio of phase 2. In Table 3.1, inclusion and matrix properties are given for homogenization examples, and the corresponding Voigt and Reuss bonds are plotted in Figure 3.2. As seen from Figure 3.2, the relation

between the Voigt bound and the volume fraction is linear, whereas the Reuss bound exhibits a non-linear relation.

Table 3.1: Material properties of homogenization examples.

Constituent	Young's Modulus [GPa]	Poisson's Ratio [-]
Inclusion	100	0.28
Matrix	3	0.3

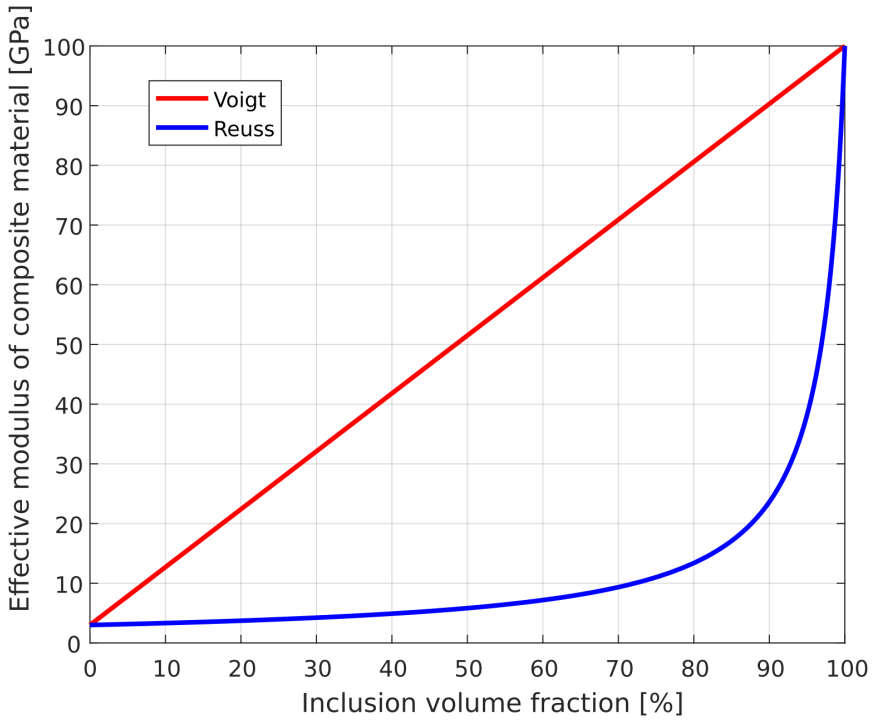


Figure 3.2: Voigt and Reuss bound comparison example.

Another well-known homogenization approach, Hashin-Shtrikman, also provides upper and lower bounds for heterogeneous materials [24]. It can be stated as the tightest bounds for the composite moduli. For a two-phase isotropic material, homogenized bulk modulus K and shear modulus μ is given in Equation 3.3, and the corresponding Hashin-Shtrikman bonds are plotted in Figure 3.3.

$$
\begin{aligned}
K_{HS}^{+} &= K_1 + \frac{\nu_2}{(K_2 - K_1)^{-1} + \frac{3\nu_1}{3K_1+4\mu_1}} \\
K_{HS}^{-} &= K_2 + \frac{\nu_1}{(K_1 - K_2)^{-1} + \frac{3\nu_2}{3K_2+4\mu_2}} \\
\mu_{HS}^{+} &= \mu_1 + \frac{\nu_2}{(\mu_2 - \mu_1)^{-1} + \frac{6(K_1+2\mu_1)\nu_1}{5\mu_1(3K_1+\mu_1)}} \\
\mu_{HS}^{-} &= \mu_2 + \frac{\nu_1}{(\mu_1 - \mu_2)^{-1} + \frac{6(K_2+2\mu_2)\nu_2}{5\mu_2(3K_2+\mu_2)}}
\end{aligned}
\tag{3.3}
$$

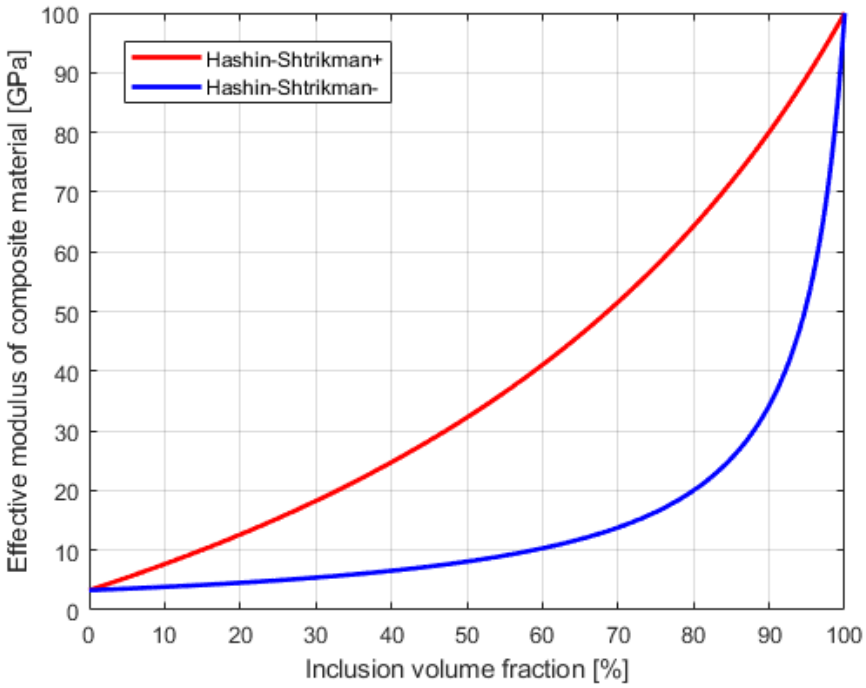


Figure 3.3: Hashin-Shtrikman bounds comparison example.

Besides these methods, several homogenization methods originated from Eshelby's inclusion-based approach [25]. Eshelby's micromechanics-based solution became the milestone for the homogenization methods. This fundamental problem determines the stress and strain fields inside and around an ellipsoidal inclusion Ω embedded in an infinite matrix. At first, Eshelby assumes an infinite linear elastic matrix $\mathbf{O}$; the stress and strain fields are uniform and zero in the matrix. Then, an ellipsoidal region Ω inside the matrix develops a uniform eigen-strain ε^*. When the ellipsoidal region is

removed from the matrix, the stress field $\boldsymbol{\sigma}$ in Ω becomes

$$\boldsymbol{\sigma} = -\mathbf{C} : \varepsilon^*, \tag{3.4}$$

where $\mathbf{C}$ elasticity tensor of matrix. Then, the strain field in Ω becomes

$$\varepsilon = \mathbf{S} : \varepsilon^*, \tag{3.5}$$

where $\mathbf{S}$ is the Eshelby tensor of the ellipsoidal region and depends on the elasticity tensor of the matrix and shape of the ellipsoidal region. Then, the stress field can be written by inserting Equation 3.5 into Equation 3.5.

$$\boldsymbol{\sigma} = \mathbf{C} : (\varepsilon - \varepsilon^*) = \mathbf{C} : (\mathbf{S} - \mathbf{I}) : \varepsilon^* \qquad \text{in} \qquad \Omega \tag{3.6}$$

.

Then, Eshelby proposes another important problem, which is known as Eshelby's inclusion-based approach; instead of the ellipsoidal region in the matrix, an inclusion is considered. Inclusion's elasticity tensor $\mathbf{C_{inc}}$ is different than the matrix. In the problem, a far-field strain $\overline{\varepsilon}$ is applied to the matrix. At this point, Eshelby decomposes the strain field as $\overline{\varepsilon} + \varepsilon$ where ε is assumed to be the same for both problems. Therefore, the strain field also becomes the same.

$$\boldsymbol{\sigma} = \mathbf{C_{inc}} : (\overline{\varepsilon} + \varepsilon) = \mathbf{C} : (\overline{\varepsilon} + \varepsilon - \varepsilon^*) \qquad \text{in} \qquad \Omega \tag{3.7}$$

ε^*, which is unknown and can be solved now by using Equation 3.7. When considering the volume of the inclusion, the composite's effective elasticity tensor can be calculated through the stress-strain relationship for the constitutive model by extending Eshelby's inclusion-based approach as a homogenization method. If the problem exhibits nonlinear behavior, more complex constitutive models are needed to describe the stress-strain relationship.

Several homogenization methods are developed using Eshelby's inclusion problem,

such as the Mori-Tanaka method used in the study [26]. Mori-Tanaka states that inclusion is embedded in a finite matrix. In the Mori-Tanaka homogenization theory, effective elasticity tensor $\mathbf{C}^{eff}$ is defined by,

$$\mathbf{C}^{eff} = \mathbf{C}^m + \sum_{\alpha=1}^{B} v_\alpha (\mathbf{C}^\alpha - \mathbf{C}^m) : \mathbf{A}^\alpha, \tag{3.8}$$

where α, B, v_α, $\mathbf{C}^m$, and $\mathbf{C}^\alpha$ respectively represent the inclusion number, the total number of inclusions, the volume fraction of the α^{th} inclusion, the fourth-order elasticity tensor of the matrix, and inclusion. The strain concentration tensor $\mathbf{A}^\alpha$ is defined as

$$\mathbf{A}^\alpha = \mathbf{A}_m^\alpha : \left[v_m \mathbb{I} + \sum_{\beta}^{B} v_\beta \mathbf{A}_m^\beta \right]^{-1}, \tag{3.9}$$

where v_m and $\mathbb{I}$ represent the volume fraction of the matrix and fourth-order identity tensor, respectively. Taking the inverse of a fourth-order tensor is explained in Appendix A. $\mathbf{A}_m^\alpha$ is defined as

$$\mathbf{A}_m^\alpha = \left[\mathbb{I} + \mathbf{S}^\alpha : (\mathbf{C}^m)^{-1} : (\mathbf{C}^\alpha - \mathbf{C}^m) \right]^{-1}, \tag{3.10}$$

In Equation 3.10, $\mathbf{S}^\alpha$ is the Eshelby tensor. For a spherical inclusion, the Eshelby tensor is defined as

$$\begin{aligned} S_{1111} = S_{2222} = S_{3333} &= \frac{7 - 5\nu_0}{15(1 - \nu_0)} \\ S_{1122} = S_{2233} = S_{3311} &= \frac{5\nu_0 - 1}{15(1 - \nu_0)} \\ S_{1212} = S_{2323} = S_{3131} &= \frac{4 - 5\nu_0}{15(1 - \nu_0)}, \end{aligned} \tag{3.11}$$

where ν_0 is the Poisson's ratio of the isotropic matrix. All other components of the Eshelby tensor are zero. Comparison of Vogit, Reuss, Hashin-Shtrikman, and Mori-

Tanaka methods for the given example are plotted in Figure 3.4.

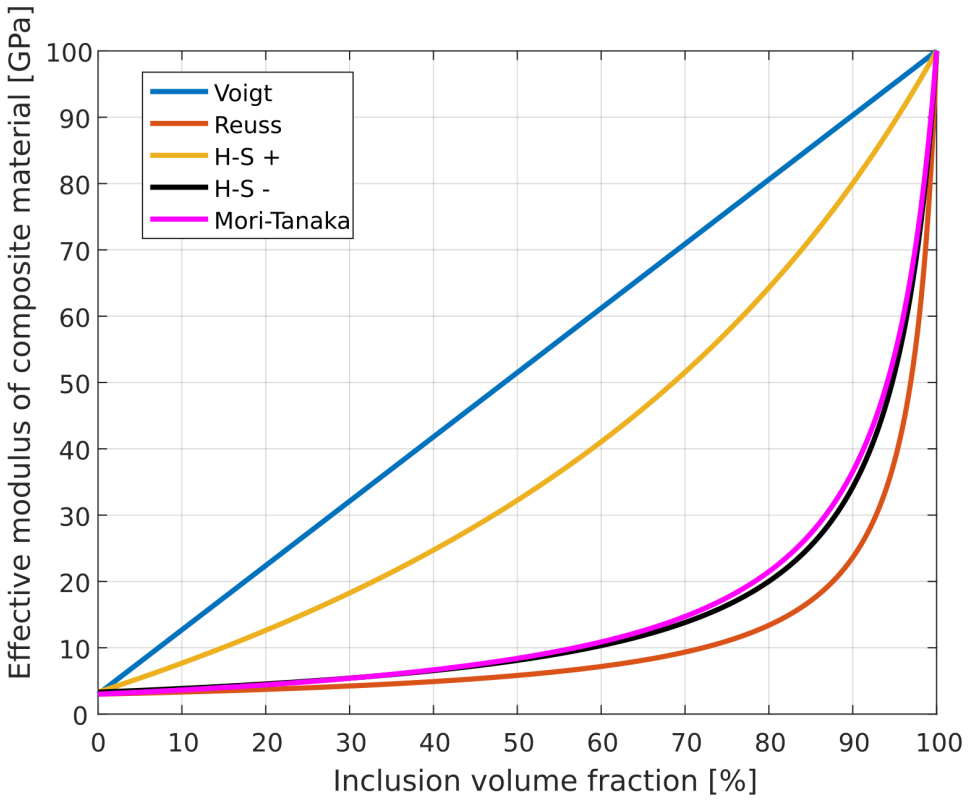


Figure 3.4: Comparison of different analytical homogenization approaches.

3.2 Computational methods

The finite element method is a computational method that promises an approximation to a physical problem by modeling the problem in the domain of finite elements. The physical problem is solved by formulating a set of equations based on governing physics with the application of appropriate boundary conditions. For the homogenization of a heterogeneous material, the effective elasticity tensor can be obtained by calculating the stress and strain fields over the domain of an RVE. Critical points of FEM based homogenization method are the construction of the RVE and the application of the appropriate boundary conditions. The model's behavior in the finite element method must reflect the original problem. After constructing the appropriate RVE for the finite element model, one should select appropriate boundary conditions.

In general, there are three different boundary conditions for computational homogenization. As stated earlier in this chapter, these are linear displacement, periodic, and uniform traction boundary conditions. After solving finite element problems, stresses, strains, and the volume of each integration point of the element are used to calculate the effective properties of the material system via the constitutive model.

In order to proceed with the finite element analysis, boundary conditions must satisfy Hill's energy principle [21], [27], [28].

$$\overline{\boldsymbol{\sigma} : \boldsymbol{\varepsilon}} = \overline{\boldsymbol{\sigma}} : \overline{\boldsymbol{\varepsilon}} \tag{3.12}$$

Let's define $\mathbf{x}$ as any coordinate point in the representative volume element of a heterogeneous material. The bar over the coordinate point $\bar{\mathbf{x}}$ denotes the coordinate point at a macroscopic level, which means volume average. Displacement field $\mathbf{u}$ in the microscopic level:

$$\mathbf{u}(\overline{\mathbf{x}}, \mathbf{x}, t) = \overline{\boldsymbol{\varepsilon}}(\overline{\mathbf{x}}, t)\mathbf{x} + \mathbf{r}(\overline{\mathbf{x}}, \mathbf{x}, t), \tag{3.13}$$

where $\bar{\varepsilon}\mathbf{x}$ and $\mathbf{r}$ are the linear and fluctuating part of the field $\mathbf{u}$ and t is time. With the assumption of no fluctuation field, macroscopic strain field $\bar{\varepsilon}$ can be defined by microscopic displacement $\mathbf{u}$, and the formulation simplifies to a compact form.

$$\int_V \nabla \mathbf{r} \ dV = \int_\Gamma \mathbf{n} \otimes \mathbf{r} \ d\Gamma = 0 \tag{3.14}$$

$$\overline{\boldsymbol{\varepsilon}} = \frac{1}{\mid V \mid} \int_V \varepsilon \ dV, \tag{3.15}$$

where V is the volume of the RVE. Similar to the macroscopic strain tensor, the macroscopic stress tensor can be described over the volume of the RVE as follows,

$$\overline{\boldsymbol{\sigma}} = \frac{1}{\mid V \mid} \int_V \sigma \ dV \tag{3.16}$$

Hill's theorem states that the above relationships are satisfied and can be derived from Hill's energy principle [21].

3.2.1 Linear Displacement Boundary Condition

Linear displacement boundary condition (Dirichlet condition [29]) defines the displacement field of the entire boundary as a linear function of the position. The displacement field on the boundaries of RVE is defined as:

$$\mathbf{u} = \langle \boldsymbol{\varepsilon}(\mathbf{u}) \rangle \mathbf{x} \quad \text{on} \quad \Gamma, \tag{3.17}$$

where $\boldsymbol{\varepsilon}(\mathbf{u})$ is the strain filed and $\mathbf{x}$ is the position vector of a point on the boundary Γ.

3.2.2 Periodic Boundary Condition

The periodic boundary condition is applicable for periodic RVEs over a medium. Application of periodic boundary conditions assumes that stresses and strains are also periodic over the periodic RVEs. To introduce the PBC, the boundary of the RVE is divided into two opposite parts, Γ^- and Γ^+, which satisfies that $\Gamma^- \cup \Gamma^+ = \Gamma$. Discretization of the RVE for PBC is illustrated in Figure 3.5. The unit normal vectors should satisfy $\mathbf{n}^- = -\mathbf{n}^+$ for each point pair placed on the opposite boundaries of the RVE. When these conditions are satisfied, PBC is defined as on the RVE:

$$\mathbf{u}^+ - \mathbf{u}^- = \langle \boldsymbol{\varepsilon}(\mathbf{x}^+ - \mathbf{x}^-) \rangle \quad \text{and} \quad \mathbf{t}^- = -\mathbf{t}^+ \quad \text{on} \quad \Gamma, \tag{3.18}$$

where $\mathbf{t}^\pm = \boldsymbol{\sigma}\mathbf{n}^\pm$ are the anti-periodic traction vectors on the opposite boundaries.

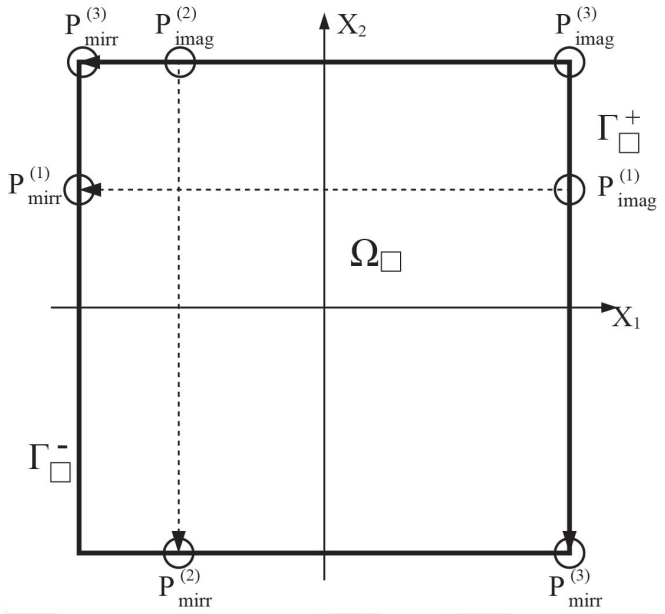


Figure 3.5: Discritization of a RVE for PBC [8].

3.2.3 Uniform Traction Boundary Condition

The uniform traction boundary condition (Neumann condition [29]) defines a stress vector field on the boundary of RVE that assumes stress is uniform inside the REVE. The stress field is defined on the RVE:

$$\boldsymbol{\sigma}\mathbf{n} = \langle\boldsymbol{\sigma}\rangle\mathbf{n} \quad \text{on} \quad \Gamma, \tag{3.19}$$

where σ is the stress tensor and $\mathbf{n}$ is the unit normal vector on the boundary Γ.
The uniform traction boundary condition gives the softest behavior, comparing all these three boundary conditions. There are studies on the comparison of these boundary conditions in the literature, and details can be found in [30], [31].

CHAPTER 4

METHODOLOGY

In this thesis, CNTs and carbon fiber are considered transversely isotropic linear elastic, while epoxy is assumed to be isotropic linear elastic as commonly employed in the literature. Material properties are taken from the study of Tsai et al. [32] and can be seen in Table 4.1. In Table 4.1, E_L, E_T, G_L, ν_L, and ν_T correspond to tensile or longitudinal elastic modulus parallel to the fiber direction, transverse elastic modulus perpendicular to the fiber direction, in-plane shear modulus parallel to the fiber direction, in-plane Poisson's ratio parallel to the fiber direction, and out-plane Poisson's ratio perpendicular to the fiber direction, respectively. Also, the definition of these engineering properties is illustrated in Figure 4.1. The FFC model consists of a unidirectional fiber, radially grown CNTs, and an epoxy matrix. CNTs' radius and length are assumed to be the same, and CNT waviness and agglomeration are not considered. CNTs are considered inclusions in the epoxy matrix. Furthermore, between the constituents, perfect bonding is assumed [33].

Table 4.1: The engineering material properties of carbon fiber, CNT, and epoxy.

Material	E_L [Pa]	E_T [Pa]	G_L [Pa]	ν_L [-]	ν_T [-]
Carbon Fiber	230×10^9	15×10^9	25×10^9	0.29	0.46
CNT	759×10^9	425×10^9	596×10^9	0.27	0.20
Epoxy	3×10^9	3×10^9	1.15×10^9	0.30	0.30

Homogenizing the FFC in a single model is computationally expensive due to the size difference of the constituents. The fiber radius is in the micro, and the CNT radius is in the nano size, which makes a size difference in the order of thousands.

Therefore, a two-step homogenization approach will be followed to understand the overall macroscopic behavior of the composite. In the first step, the interphase region consisting of a polymer matrix and radially aligned CNTs is homogenized using the micromechanics-based Mori-Tanaka method. After obtaining the homogenized properties of the interphase, the 3-phase FFC will be homogenized using the Finite Element Method. ABAQUS and MATLAB programs are used to implement the homogenization method.

4.1 Computational Homogenization Approach

The Helmholtz free energy function Ψ defines the constitutive model of elasticity, and the fourth-order elasticity tensor is obtained through the derivative of the energy function for hyperelastic materials:

$$\mathbf{C} = \partial^2_{\boldsymbol{\varepsilon}\boldsymbol{\varepsilon}} \Psi(\boldsymbol{\varepsilon}). \tag{4.1}$$

The fourth-order elasticity tensor has 81 components. Due to the major symmetry as in Equation 4.2 and minor symmetry as in Equation 4.3 of the tensor, the number of independent coefficients reduces to 21 for the most general anisotropic material [34].

$$C_{ijkl} = C_{klij} \tag{4.2}$$

$$\begin{aligned} C_{ijkl} &= C_{jikl} \\ C_{ijkl} &= C_{ijlk} \end{aligned} \tag{4.3}$$

In order to compute these 21 constants, 21 equations are needed. As the material changes monoclinic, orthotropic, transversely isotropic, and isotropic, the number of the independent elastic constants reduces to 13, 9, 5, and 2, respectively. The stress-strain relation for anisotropic linear elastic material in Voigt notation reads as follows:

$$\begin{bmatrix}\sigma_{11}\\ \sigma_{22}\\ \sigma_{33}\\ \sigma_{23}\\ \sigma_{13}\\ \sigma_{12}\end{bmatrix} = \begin{bmatrix} C_{11} & C_{12} & C_{13} & C_{14} & C_{15} & C_{16} \\ & C_{22} & C_{23} & C_{24} & C_{25} & C_{26} \\ & & C_{33} & C_{34} & C_{35} & C_{36} \\ & & & C_{44} & C_{45} & C_{46} \\ & & & & C_{55} & C_{56} \\ sym & & & & & C_{66} \end{bmatrix} \begin{bmatrix}\varepsilon_{11}\\ \varepsilon_{22}\\ \varepsilon_{33}\\ 2\varepsilon_{23}\\ 2\varepsilon_{13}\\ 2\varepsilon_{12}\end{bmatrix} \tag{4.4}$$

For a linear elastic isotropic material, the stress-strain relation in Voigt notation simplifies as:

$$\begin{bmatrix}\sigma_{11}\\ \sigma_{22}\\ \sigma_{33}\\ \sigma_{23}\\ \sigma_{13}\\ \sigma_{12}\end{bmatrix} = \begin{bmatrix} C_{11} & C_{12} & C_{12} & 0 & 0 & 0 \\ & C_{11} & C_{12} & 0 & 0 & 0 \\ & & C_{11} & 0 & 0 & 0 \\ & & & \frac{C_{11}-C_{12}}{2} & 0 & 0 \\ & & & & \frac{C_{11}-C_{12}}{2} & 0 \\ sym & & & & & \frac{C_{11}-C_{12}}{2} \end{bmatrix} \begin{bmatrix}\varepsilon_{11}\\ \varepsilon_{22}\\ \varepsilon_{33}\\ 2\varepsilon_{23}\\ 2\varepsilon_{13}\\ 2\varepsilon_{12}\end{bmatrix} \tag{4.5}$$

In this study, fiber and interphase, i.e., the region around the fiber consisting of CNTs and the matrix, are considered transversely isotropic materials, and the matrix is isotropic. A fuzzy fiber composite system shows transversely isotropic material behavior. The stress-strain relation for a transversely isotropic material in the Voigt notation is

$$\begin{bmatrix}\sigma_{11}\\ \sigma_{22}\\ \sigma_{33}\\ \sigma_{23}\\ \sigma_{13}\\ \sigma_{12}\end{bmatrix} = \begin{bmatrix} C_{11} & C_{12} & C_{12} & 0 & 0 & 0 \\ & C_{22} & C_{23} & 0 & 0 & 0 \\ & & C_{22} & 0 & 0 & 0 \\ & & & \frac{C_{22}-C_{23}}{2} & 0 & 0 \\ & & & & C_{55} & 0 \\ sym & & & & & C_{55} \end{bmatrix} \begin{bmatrix}\varepsilon_{11}\\ \varepsilon_{22}\\ \varepsilon_{33}\\ 2\varepsilon_{23}\\ 2\varepsilon_{13}\\ 2\varepsilon_{12}\end{bmatrix}. \tag{4.6}$$

The number of independent elastic constants for a transversely isotropic system is five, so five equations are needed to find the constants. Normal loading in the fiber

direction ($\varepsilon_{11} \neq 0, \varepsilon_{22} = \varepsilon_{33} = \varepsilon_{23} = \varepsilon_{13} = \varepsilon_{12} = 0$) is applied to the finite element model to compute the C_{11} and C_{12}. Normal loading in the transverse direction ($\varepsilon_{22} \neq 0, \varepsilon_{11} = \varepsilon_{33} = \varepsilon_{23} = \varepsilon_{13} = \varepsilon_{12} = 0$) is applied to calculate C_{22} and C_{23}. Moreover, shear loading parallel to the fiber direction ($\varepsilon_{13} \neq 0, \varepsilon_{11} = \varepsilon_{22} = \varepsilon_{33} = \varepsilon_{23} = \varepsilon_{12} = 0$) is applied to compute the last unknown elastic coefficient, C_{55}. Note that load cases different from the one described here can be chosen to calculate the elastic constants. In this study, three load cases, explained above and given in Equation 4.7, will be applied in FEA to calculate the elastic constants.

$$\overline{\boldsymbol{\varepsilon}} = \begin{bmatrix} a & 0 & 0 \\ 0 & 0 & 0 \\ 0 & 0 & 0 \end{bmatrix}, \begin{bmatrix} 0 & 0 & 0 \\ 0 & a & 0 \\ 0 & 0 & 0 \end{bmatrix}, \begin{bmatrix} 0 & 0 & 0 \\ 0 & 0 & a \\ 0 & a & 0 \end{bmatrix} \tag{4.7}$$

In Equation 4.7, $\overline{\boldsymbol{\varepsilon}}$ is the externally applied homogenized strain. After completing the finite element analysis, each integration point's stresses, strains, and volume are used to calculate homogenized stress and strain tensors as shown in Equation 4.8.

$$\begin{aligned} \overline{\boldsymbol{\sigma}} &= \frac{\sum_{n=1}^{NI} \boldsymbol{\sigma_n} V_n}{\sum_{n=1}^{NI} V_n} \\ \overline{\boldsymbol{\varepsilon}} &= \frac{\sum_{n=1}^{NI} \boldsymbol{\varepsilon}_n V_n}{\sum_{n=1}^{NI} V_n}, \end{aligned} \tag{4.8}$$

where NI is the total number of the integration points in the FE model, V_n is the volume of the integration point n, $\boldsymbol{\sigma_n}$ and $\boldsymbol{\varepsilon_n}$ are the stress and strain tensors at the integration point n.

In the finite element analysis, isoparametric elements, which help the numerical integration of element equations, are used. Let us define an orthogonal natural coordinate system of isoparametric elements as w_1, w_2, and w_3 where the each axis ranges from -1 to 1. The volume of an infinitesimal element can be written as

$$dV = dxdydz = Jdw_1dw_2dw_3, \tag{4.9}$$

where J is the Jacobian of the transformation of the infinitesimal volume in terms of the natural coordinates w_1, w_2, and w_3 to that calculated using the physical global

coordinates of finite elements x, y, and z. Then, the Jacobian J is mathematically defined as

$$J = \begin{vmatrix} \frac{\partial x}{\partial w_1} & \frac{\partial x}{\partial w_2} & \frac{\partial x}{\partial w_3} \\ \frac{\partial y}{\partial w_1} & \frac{\partial y}{\partial w_2} & \frac{\partial y}{\partial w_3} \\ \frac{\partial z}{\partial w_1} & \frac{\partial z}{\partial w_2} & \frac{\partial z}{\partial w_3} \end{vmatrix}. \tag{4.10}$$

Then, the volume of a finite element can be expressed as

$$\iiint_{V_{element}} dxdydz = \iiint_{W} Jdw_1dw_2dw_3. \tag{4.11}$$

The integral given in Equation 4.11 is calculated numerically in a finite element analysis by the Gauss-Legendre quadrature. For a tri-linear hexagonal element, the volume of an element reads

$$V_{element} = \sum_{n=1}^{8} J_n\omega_n, \tag{4.12}$$

where ω_n is the Gaussian weighting factor of the integration point n. Therefore, the volume of the integration points V_n in Equation 4.8 becomes

$$V_n = J_n w_n. \tag{4.13}$$

Five unknown independent elasticity tensor constants are calculated with homogenized stress and strain tensors via the constitutive model. C_{11} and C_{12} can be calculated by substituting the calculated average stresses and strains from Equation 4.8 for the normal loading case in the fiber direction. Equation 4.6 simplifies to Equation 4.14 and can be calculated easily.

$$\begin{aligned} \overline{\sigma}_{11} &= C_{11}\overline{\varepsilon}_{11} \\ \overline{\sigma}_{22} &= C_{12}\overline{\varepsilon}_{11} \\ \overline{\sigma}_{33} &= C_{12}\overline{\varepsilon}_{11} \end{aligned} \tag{4.14}$$

Similarly, for the normal loading case in the transverse direction, C_{22} and C_{23} can be calculated by substituting the calculated average stresses and strains. Equation 4.6 simplifies to Equation 4.15.

$$\begin{aligned} \overline{\sigma}_{11} &= C_{12}\overline{\varepsilon}_{22} \\ \overline{\sigma}_{22} &= C_{22}\overline{\varepsilon}_{22} \\ \overline{\sigma}_{33} &= C_{23}\overline{\varepsilon}_{22} \end{aligned} \tag{4.15}$$

The same steps are followed to calculate the elastic constant C_{55} for the simple shear loading parallel to the fiber direction. Equation 4.6 simplifies to Equation 4.16.

$$\overline{\sigma}_{13} = C_{55}\overline{\varepsilon}_{13} \tag{4.16}$$

Engineering material constants can be found by decomposing the compliance tensor $\mathbf{S}$. The definition of the engineering properties for a transversely isotropic material can be seen in Figure 4.1. The compliance tensor is the inverse of the elasticity tensor $\mathbf{C}$.

$$\mathbf{S} = \mathbf{C}^{-1} \tag{4.17}$$

Compliance tensor can be calculated easily by inverting the elasticity tensor as stated in Equation 4.17 [35]. The engineering constants can be found by decomposing the compliance tensor. The compliance tensor for a transversely isotropic material reads as follows:

$$\mathbf{S} = \begin{bmatrix} \frac{1}{E_1} & \frac{-\nu_{12}}{E_1} & \frac{-\nu_{12}}{E_1} & 0 & 0 & 0 \\ & \frac{1}{E_2} & \frac{-\nu_{23}}{E_2} & 0 & 0 & 0 \\ & & \frac{1}{E_2} & 0 & 0 & 0 \\ & & & \frac{1}{G_{23}} & 0 & 0 \\ & & & & \frac{1}{G_{13}} & 0 \\ sym & & & & & \frac{1}{G_{13}} \end{bmatrix}. \tag{4.18}$$

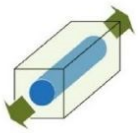
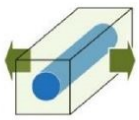
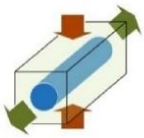
Tensile elastic modulus	Transverse elastic modulus	Out-plane Poisson's ratio	In-plane Poisson's ratio	Out-plane shear modulus	In-plane shear modulus
					
E_L	E_T	ν_T	ν_L	G_T	G_L

Figure 4.1: Engineering constants of a transversely isotropic material [9].

4.2 Homogenization of the Interphase

CNT interphase region has a graded structure because the volume fraction of the CNTs decreases as the distance from the fiber surface increases. Therefore, homogenizing the interphase with FEM requires a complex model. A comparison study between the Mori-Tanaka method and FEM is conducted for the homogenization of the interphase.

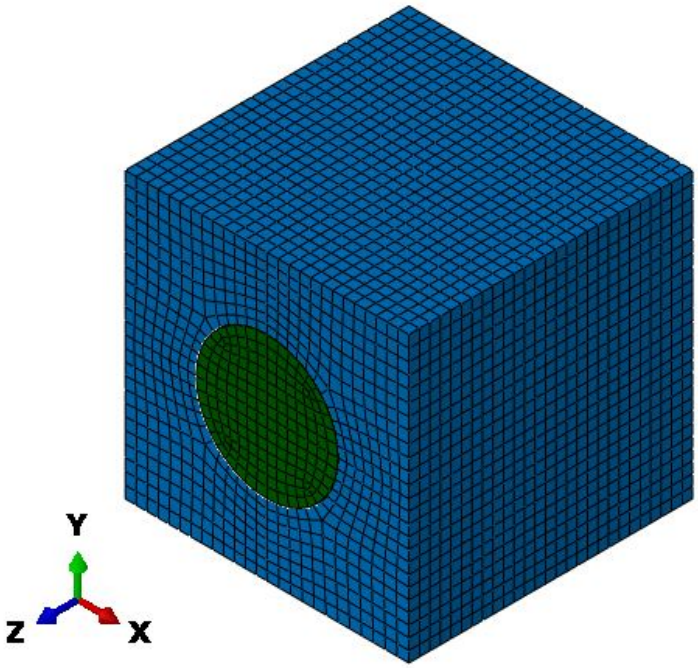


Figure 4.2: FE model of RVE of CNT for the aspect ratio of CNT of 2.

Three different FE models are constructed with a single CNT fiber. FE model of the CNT reinforced epoxy is shown in Figure 4.2. The aspect ratio of CNT is stated in Equation 4.19:

$$AR = \frac{r_{CNT}}{l_{CNT}}, \tag{4.19}$$

where r_{CNT} is the CNT radius, and l_{CNT} is the CNT length. In the FE models, only CNT lengths vary while keeping the other parameters constant. In order to calculate the effective elastic coefficients of the interphase, three different loadings stated in Equation 4.7 are applied as in Table 4.2.

Table 4.2: Load cases applied with linear displacement boundary condition to the RVE consisting of single CNT and epoxy matrix.

Loading Case	Strain	Stress (Response)
Axial Loading (11)	$\{\varepsilon_{11}, 0, 0, 0, 0, 0\}$	$\{\sigma_{11}, \sigma_{22}, \sigma_{33}, 0, 0, 0\}$
Transverse Loading (22)	$\{0, \varepsilon_{22}, 0, 0, 0, 0\}$	$\{\sigma_{11}, \sigma_{22}, \sigma_{33}, 0, 0, 0\}$
Simple Shear Loading (13)	$\{0, 0, 0, 0, \gamma_{13}, 0\}$	$\{0, 0, 0, 0, \tau_{13}, 0\}$

CNTs are cylindrical inclusions in the interphase. Thus, the Eshelby tensor for cylindrical inclusion in the isotropic matrix should be used in the equations. As depicted in Chapter 3, the Mori-Tanaka method is followed. In Equation 3.10, $\mathbf{S}^{\alpha}$ is the Eshelby tensor [36]. In this study, the Mori-Tanaka method is implemented for cylindrical CNT. Thus, the Eshelby tensor for cylindrical inclusion in the isotropic matrix should be used in the equations. For a needle or circular cylinder, the components of the Eshelby tensor are defined as

$$\begin{aligned} S_{1111} &= 0 \\ S_{2222} = S_{3333} &= \frac{5 - \nu_0}{8(1 - \nu_0)} \\ S_{2233} = S_{3322} &= \frac{4\nu_0 - 1}{8(1 - \nu_0)} \\ S_{2211} = S_{3311} &= \frac{\nu_0}{2(1 - \nu_0)} \end{aligned} \tag{4.20}$$

$$S_{1122} = S_{1133} = 0$$

$$S_{2323} = \frac{3 - 4\nu_0}{8(1 - \nu_0)}$$

$$S_{1212} = S_{1313} = \frac{1}{4},$$

where ν_0 is the Poisson's ratio of the isotropic matrix.

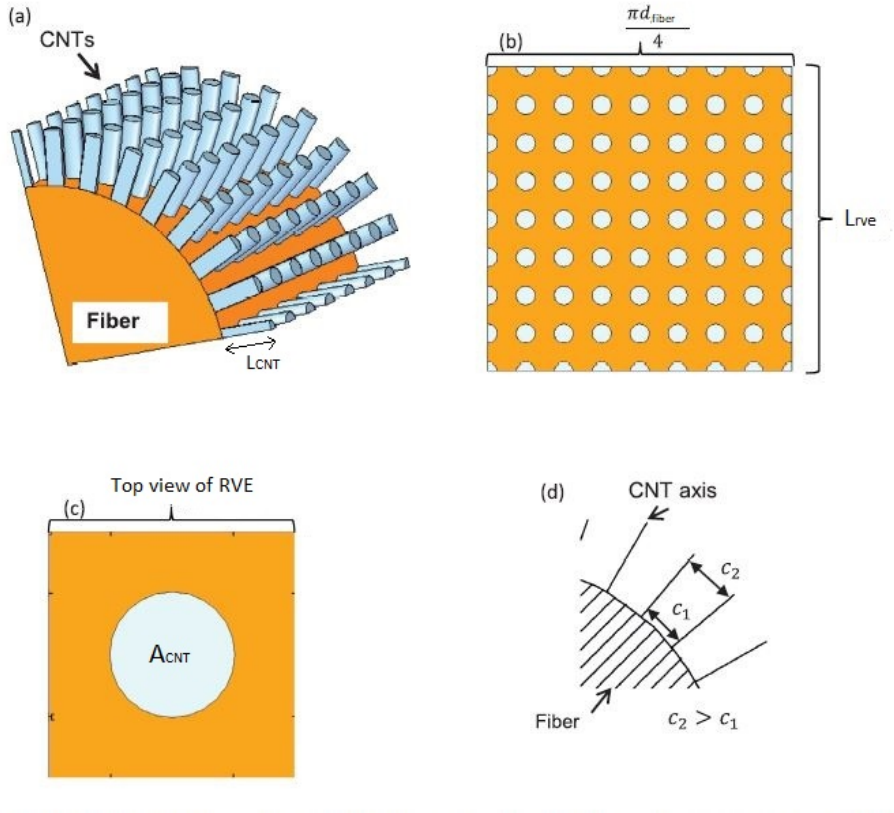


Figure 4.3: Representation of FFC: (a) 3D RVE of FFC; (b) CNTs on fiber surface from top view; (c) RVE of a single CNT; (d) Reduction in CNT volume fraction representation [10].

The Mori-Tanaka method calculates the effective elasticity tensor with the volume fraction of the inclusion. As mentioned before, the local volume fraction of the CNTs changes in the interphase. The local volume fraction of the CNTs is calculated by the pre-known total CNT volume fraction in the composite for a given RVE. The total number of CNTs NO_{CNT} is calculated as,

$$NO_{CNT} = \frac{\nu_{CNT} V_{RVE}}{A_{CNT}\, l_{CNT}}, \tag{4.21}$$

where ν_{CNT} is the CNT volume fraction in the FFC, V_{RVE} is the volume of the RVE representing the interphase region, A_{CNT} is the cross-sectional area of a single CNT, and l_{CNT} is the CNT length. The local CNT volume fraction becomes

$$\nu_{CNT_{local}}(r) = \frac{A_{CNT} NO_{CNT}}{2\pi r l_{RVE}}, \tag{4.22}$$

where l_{RVE} is the RVE length as defined in Figure 4.3, and r is the radial distance from the center of the carbon fiber.

Table 4.3: Comparison of Mori-Tanaka and FE results for the interphase region.

	C_{11} [GPa]	C_{12} [GPa]	C_{22} [GPa]	C_{23} [GPa]	C_{55} [GPa]
FEA (AR=2)	7.404	2.701	6.501	2.632	6.260
FEA (AR=6)	7.394	2.531	6.092	2.463	4.009
FEA (AR=20)	7.389	2.446	5.881	2.375	2.552
Mori-Tanaka	7.407	2.409	5.699	2.428	2.050

CNTs have a radius of 7.1 nanometers, and 2 micrometers length is used; the aspect ratio of the CNT becomes approximately 280. In the FE models, the aspect ratios of the inclusions are 2, 6, and 20. As the inclusion aspect ratio increases, effective elastic constants converge to the Mori-Tanaka results, as presented in Table 4.3. The elastic constant C_{55} is affected far too much as the length of the RVE increases. The other elastic constants are not much affected by the length of the RVE as observed in C_{55}. Indices of the elastic constants, given in Table 4.3, represent the cylindrical coordinate system of the interphase. Indices 1, 2, and 3 can be replaced by r, θ, and z, which are the radial direction perpendicular to the fiber surface, the angular counterclockwise direction from the radial direction, and the direction of the carbon fiber. It is concluded from the results for the homogenization of the interphase the Mori-Tanaka method gives accurate results. In terms of computation cost, the Mori-Tanaka method is very effective compared to FEM. Because of the functionally graded structure of the interphase, for every integration point in the interphase region, homoge-

nized properties must be calculated according to the distance from the fiber surface. In the Mori-Tanaka method, only the inclusion volume fraction must be calculated for the integration points. In FEA, a new RVE must be constructed and analyzed. By considering these, the Mori-Tanaka method provides a cost-effective solution for the homogenization of the interphase.

4.3 Homogenization of the FFC

The choice of boundary condition type is crucial in the homogenization of the FFC. Periodic boundary conditions are the most commonly applied conditions for periodic RVEs. Application of the periodic boundary condition for this study is tough because of the complexity and the mesh density of the RVE. Therefore, linear displacement boundary conditions are employed. A parametric study is conducted to obtain an appropriate RVE to homogenize the FFC with linear displacement boundary conditions. Details of the parametric study are given in Appendix B. As the result of the parametric study, a long square prism is constructed as the RVE of the FFC, as shown in Figure 4.4. The length of the prism is determined from the parametric study conducted.

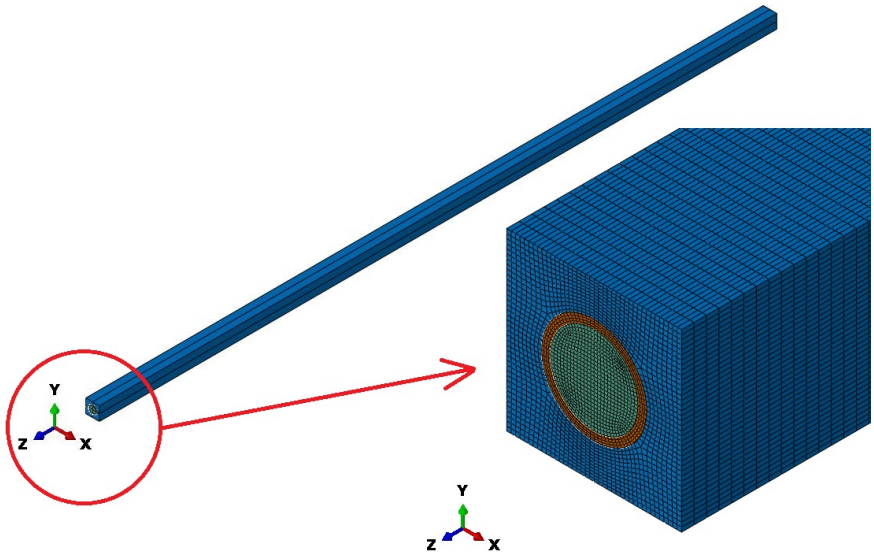
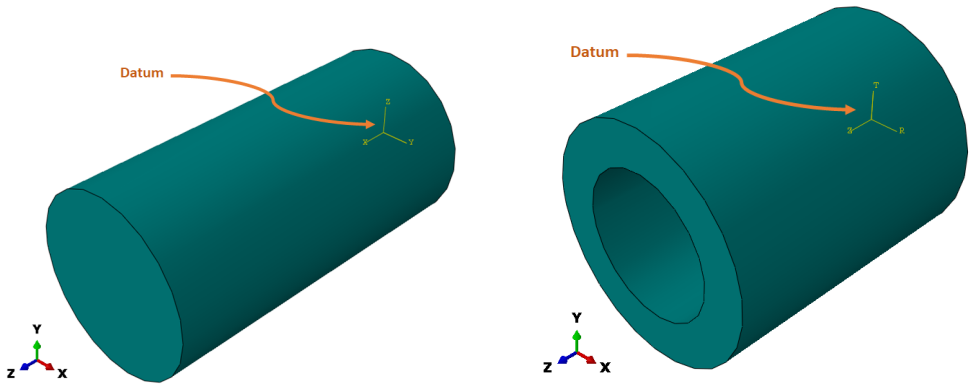


Figure 4.4: FE model of the FFC.

The FE model is created in the ABAQUS. For the meshing of the model, the first-order linear hexagonal brick elements (C3D8) are used for all phases of the FFC. For the graded interphase region, a FORTRAN code is developed, given in Appendix C, to define the material properties of the graded region in the ABAQUS USDFL subroutine [37]. Results from the Mori-Tanaka method are implemented as material properties in the ABAQUS finite element solver for every integration point of finite elements located in the interphase region. Since the FFC has a transversely isotropic structure, three different loadings are applied: normal loading in the fiber direction, normal loading in the transverse direction, and simple shear loading parallel to the fiber direction. After completing the finite element analysis, each integration point's stresses, strains, and volume are exported as an ABAQUS report file. Finally, a subroutine in MATLAB, given in Appendix D, is written to calculate the homogenized properties of the FFC with the ABAQUS report file.

Material properties are defined in the material coordinate system; all three phases have different characteristics. A datum coordinate system is created, as shown in Figure 4.5, to define transversely isotropic material properties for the carbon fiber. Then, using the datum, material orientation is assigned.

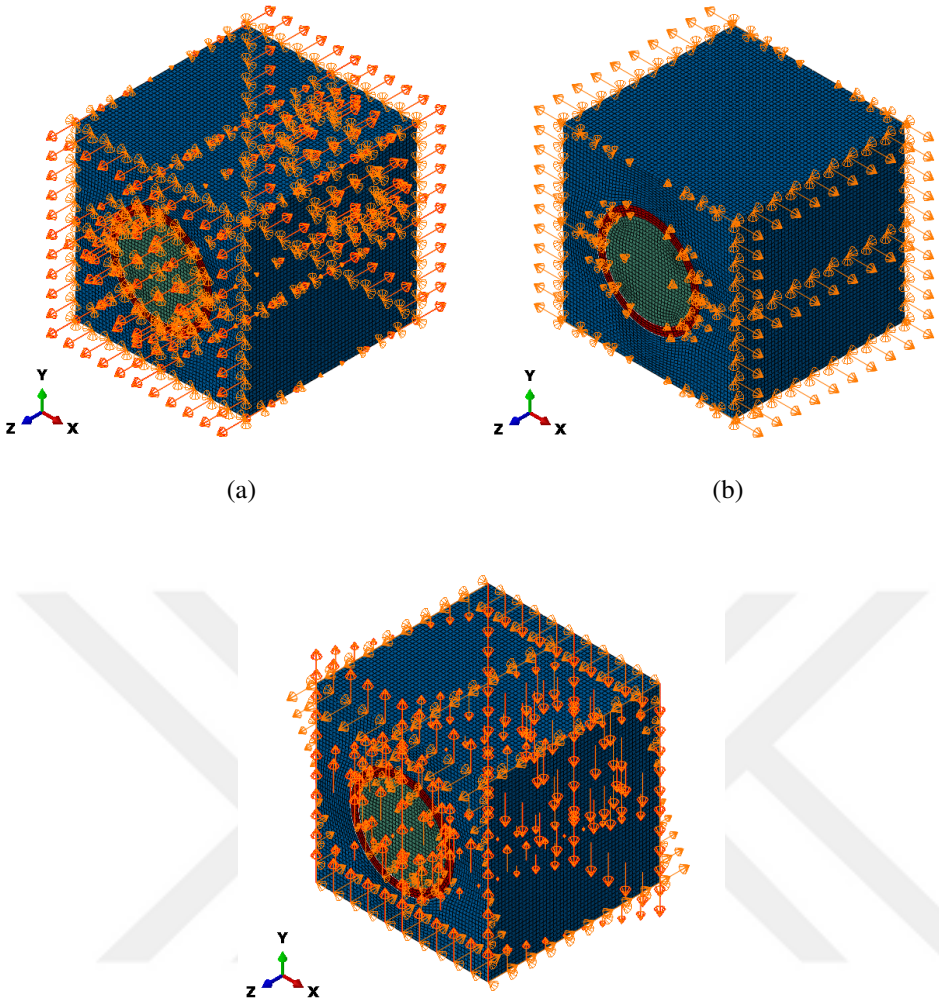


(a) (b)

Figure 4.5: Defining datum coordinate systems to the fiber (a) and the interphase (b) in ABAQUS.

Nine engineering constants are defined through the defined material orientation. Hence, carbon fiber is a transversely isotropic material; only five of the defined nine engineering constants are independent. Same as the carbon fiber, the same steps are followed for the interphase. However, the interphase's material orientation differs from that of fiber. Interphase has a transversely isotropic structure in a cylindrical coordinate system. So, a cylindrical datum coordinate system is created, and material orientation is assigned through the datum.

Fuzzy fiber composites exhibit transversely isotropic material properties at the macroscopic level [38]. Therefore, three load cases, as in Equation 4.7, are applied to the finite element model. These load cases are applied in ABAQUS as linear displacement boundary conditions, as illustrated in Figure 4.6. Applied boundary conditions are illustrated on the cubic RVE instead of the actual long RVE, as in Figure 4.4, for better visualization.



(a) (b)

(c)

Figure 4.6: Linear displacement boundary conditions in ABAQUS. (a) Normal loading in the fiber direction. (b) Normal loading in the transverse direction. (c) Simple shear loading parallel to the fiber direction.

All the boundaries must be prescribed to apply the DBC correctly. BC is applied to all surface nodes of the RVE as a function of the coordinates of the nodes. All these nodes are restricted in three directions.

After completing finite element analysis, each integration point's stresses, strains, and point volume are exported to proceed with the computational homogenization step. Since the ABAQUS finite element solver gives the results in the material coordinate

system, all results must be transformed into a global coordinate system. The transformation step is performed inside the ABAQUS before the results are exported as an ABAQUS report file. Schematic procedures of the two-step computational homogenization of the FFC are given in Figure 4.7

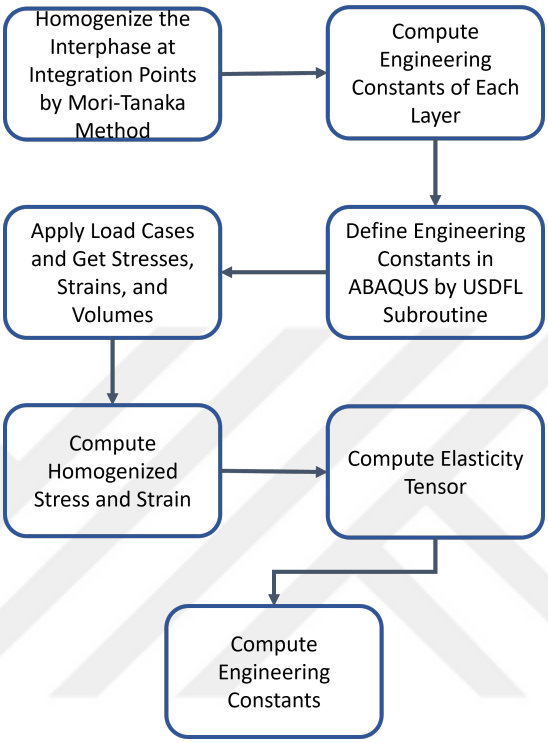


Figure 4.7: Schematic procedures of the two-step computational homogenization of the FFC.

CHAPTER 5

RESULTS

This chapter shows and discusses the results of the given FFC example. The two-step computational homogenization approach is compared with homogenization approaches from the literature. Homogenized mechanical properties of the FFC are plotted. Parametric studies of CNT volume fraction, CNT length, and fiber volume fraction are studied, and the effects of the parameters are presented. As discussed, the interphase's CNT volume fraction is variable, making the interphase a graded region. The change in the local volume fraction of the CNTs can be seen in Figure 5.1.

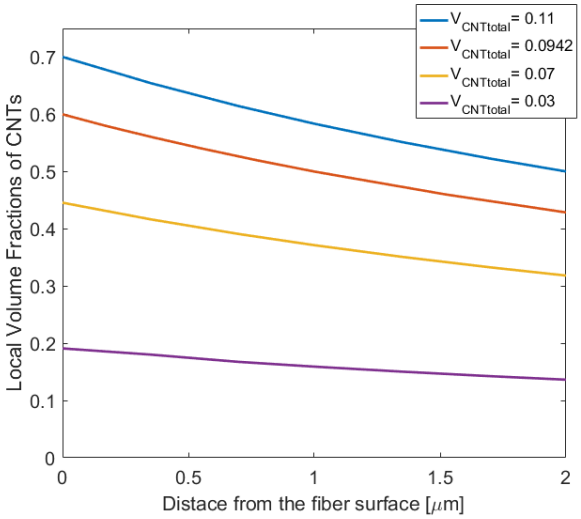


Figure 5.1: Variation of local volume fraction of CNTs in interphase as a function of distance from the fiber surface.

The vertical axis corresponds to the CNT volume fraction in the interphase region, while $V_{CNTtotal}$ is the volume fraction of CNTs in the entire composite. The local volume fractions of CNTs are calculated for the fiber volume fraction of 20% and

radius of 5 micrometers. As the local volume fraction of CNT decreases, effective engineering constants of the interphase decrease. Because of that, defining material properties for this graded region requires further work. As explained in Chapter 4, the ABAQUS USDFL subroutine is used to define the graded homogenized properties of element integration points.

The interphase region has a transversely isotropic structure in a cylindrical coordinate system (R,θ,Z). Axis-R, which defines the transverse isotropy, is parallel to the normal vector from the fiber surface to the matrix, θ is the angle between axis-2 of the FFC cartesian coordinate system and axis-R, and axis-Z coincides with the fiber direction. The definition of the interphase's cylindrical coordinate system is explained for a better understanding of the effective engineering constants of the interphase shown in Figure 5.2.

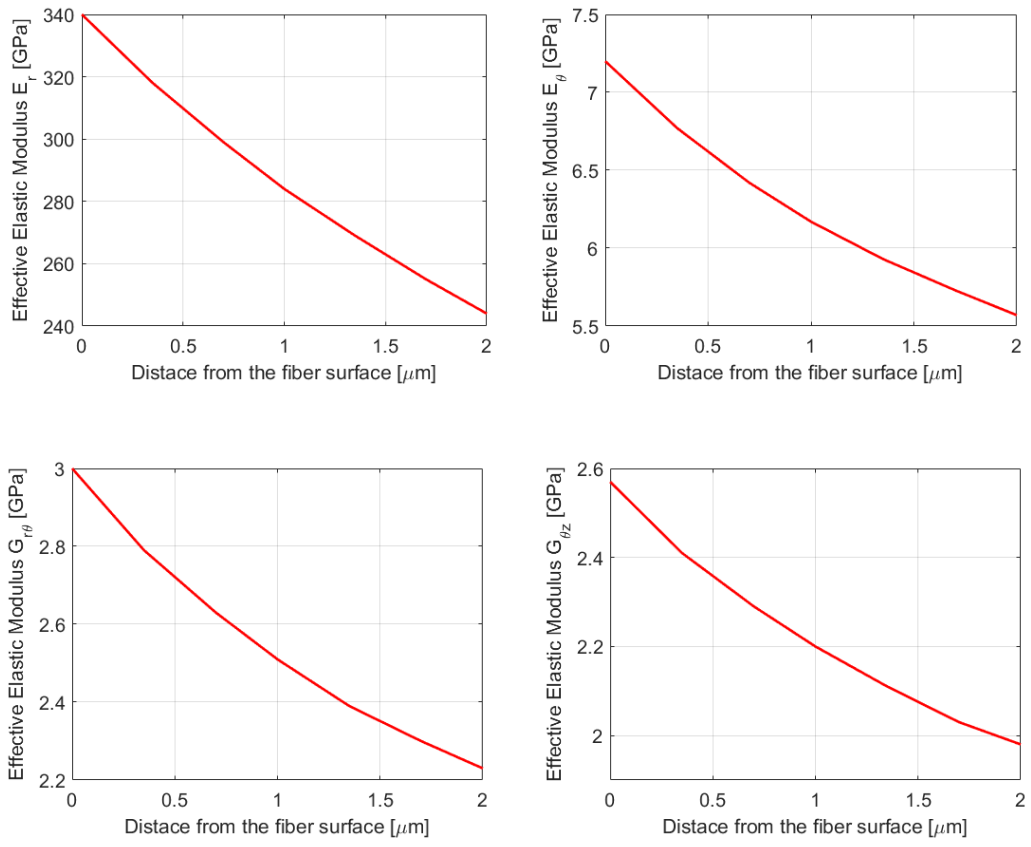


Figure 5.2: Effective interphase properties for total CNT volume fraction of 7% and fiber radius of 5 micrometers.

Three loading cases are applied in ABAQUS, as explained in Chapter 4. Undeformed and deformed shapes of the cubic RVE are shown in Figure 5.3.

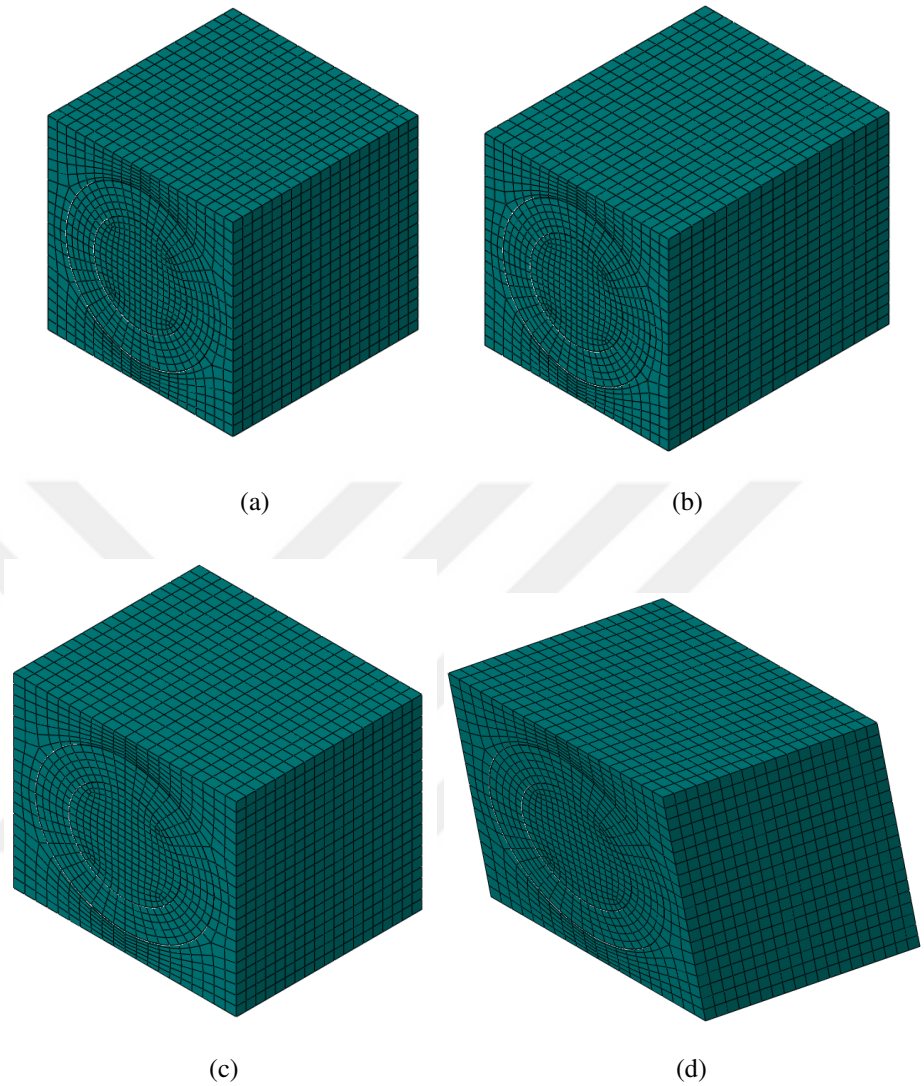


Figure 5.3: Illustration of undeformed and deformed shapes of the cubic RVE. (a) Undeformed RVE. (b) Normal loading in the fiber direction. (c) Normal loading in the transverse direction. (d) Simple shear loading parallel to the fiber direction.

5.1 Comparison with Literature

In this section, the results of the proposed two-step computational homogenization approach are compared with the literature studies.

5.1.1 Comparison with Micromechanical and Computational Approaches

The results of the proposed two-step computational homogenization approach and Cheng et al. [9] micromechanical and computational approaches are compared. In Figure 5.4, effective normalized engineering constants are presented. The horizontal axes in Figure 5.4 are the local volume fraction of CNT in the interphase. The elastic and shear moduli are normalized with respect to the carbon fiber-reinforced composite without any CNT growth on the fiber. E_1, E_2, G_{12}, and G_{23} are the fiber direction elastic modulus, transverse elastic modulus, shear modulus parallel to the fiber direction, and shear modulus perpendicular to the fiber direction, respectively. The study of Cheng et al. [9] includes a hierarchical homogenization approach extended from the Mori-Tanaka method. The number of CNTs is constant in the models. As the volume fraction of CNT increases; therefore, the length of the CNT increases where the interphase thickens. Normalized elastic constants are calculated as in Equation 5.1.

$$\beta_{normalized} = \frac{\beta_{\nu_{CNT}}}{\beta_{\nu_{CNT=0}}}, \tag{5.1}$$

where $\beta_{\nu_{CNT}}$ is any property where the CNT volume fraction is any value other than zero, i.e., the case of an FFC and $\beta_{\nu_{CNT=0}}$ is any property where the CNT volume fraction is equal to zero, i.e., the case of a classical fiber-reinforced composite.
In the two-step computational homogenization of the FFC, the material properties presented in Table 4.1 are used. The results are obtained for a fiber volume fraction of 20% and a CNT radius of 7.1 nanometers, as presented in Table 5.1.

Table 5.1: The parameters used in the comparison with the literature study with the fiber radius of 5 micrometers.

Parameter	**Value**
Fiber volume fraction ν_f	20% [-]
CNT radius r_{CNT}	7.1 [$\mathrm{n}m$]
CNT length l_{CNT}	2 [μm]

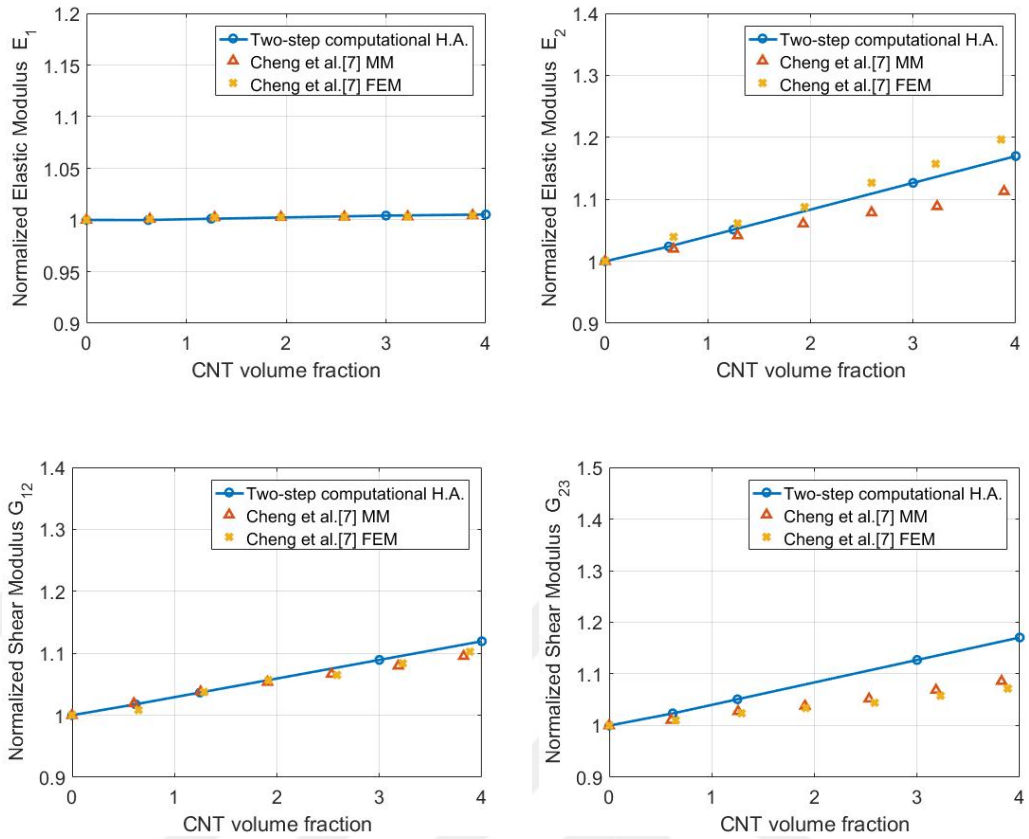


Figure 5.4: Comparison of the results obtained by two-step homogenization approach and Cheng et al. [9] (hierarchical homogenization- MM and FEM).

The results show very good agreement between the two-level computational homogenization approach and Cheng et al. [9] analytical and computational results. As seen from Figure 5.4, the effect of grafting CNTs on the fiber surface on E_1 is negligible. It has significant effects on the transverse elastic modulus and shear modulus. The two-step homogenization approach slightly overestimates the normalized shear modulus G_{23} compared to the literatıre results. The Mori-Tanaka method is used for homogenization in the study of Cheng et al. [9]. In the model, Eshelby tensor for cylindrical inclusion is used for the Mori-Tanaka method. The Eshelby tensor for cylindrical inclusion is the extension of the Eshelby tensor for ellipsoidal inclusion, which assumes that one of the lengths of the semi-axes of the ellipsoid goes to infinity to obtain the cylindrical shape, which means in the Mori-Tanaka method, inclusion goes to infinity. In the two-step computational homogenization method, RVE is con-

structed as the fiber is a finite inclusion. This could be one of the reasons for the differences in the results.

5.1.2 Comparison with Experimental Study

The results of the two-step computational homogenization approach are compared with the results of the experimental study of Kulkarni et al. [1]. For the FFC specimen, IM7 carbon fibers and Epon862 polymer matrix are used. The specimen is prepared for testing with a carbon fiber volume fraction of 41% and a CNT volume fraction of 2%. Uniaxial loading in the transverse direction is applied to the specimen in order to calculate transverse elastic modulus. The transverse elastic modulus obtained from the testing is compared with the traditional carbon fiber-reinforced polymer. The engineering constants of the carbon-reinforced polymer are taken from the study of Shan and Chou [2]. The results of the experimental study show that the elastic modulus in the transverse direction of FFC increases by 31% compared to the carbon fiber-reinforced composite. The result of the experimental study is given in Table 5.2.

Table 5.2: Transverse elastic modulus obtained from experimental study [1] and [2].

Composite	Experimental Data $E_2[GPa]$
FFC	10.2
FRP	7.8

The engineering properties of the CNTs for the experimental study are not given in the study of Kulkarni et al. [1], and the engineering constants of the matrix are different in both studies. The engineering properties of the constituents used in the two-step computational homogenization approach are given in Table 5.3.

Table 5.3: The engineering material properties of carbon fiber, CNT, and epoxy for the study of comparison with literature.

Material	E_L [Pa]	E_T [Pa]	G_L [Pa]	ν_L [-]	ν_T [-]
Carbon Fiber (IM7)	294×10^9	18.5×10^9	25×10^9	0.27	0.30
CNT	759×10^9	425×10^9	596×10^9	0.27	0.20
Epoxy (Epon862)	3×10^9	3×10^9	1.15×10^9	0.30	0.30

The length of CNTs is not defined in the experimental study. Therefore, three different RVEs are constructed for the CNT lengths of 1, 1.5, and 2 micrometers. Results of the two-step computational homogenization approach are given in Table 5.4

Table 5.4: Transverse elastic moduli of FFCs with CNT volume fraction of 2% and FRP obtained from the two-step computational homogenization approach.

Composite	Numerical Data $E_2[GPa]$
FFC (CNT length of $1\mu m$)	7.03
FFC (CNT length of $1.5\mu m$)	7.70
FFC (CNT length of $2\mu m$)	8.58
FRP	5.97

Results show that the grafting of CNTs on the surface of the fiber increases the elastic modulus in the transverse direction. Considering the enhancement in the elastic modulus E_2, different CNT lengths have different effects. Elastic modulus E_2 increased by 18%, 29%, and 44% for the CNT lengths of 1, 1.5, and 2 micrometers, respectively. Comparing the experimental and the numerical studies, the results are different. The exact material properties are not defined in the experimental studies. Hence, approximate values are taken from the literature. Because of that, there are differences in the results. But when comparing percentage change in the elastic modulus in the transverse direction, the two-step computational homogenization approach for the CNT length of 1.5 micrometers (29% increase) and the experimental study

(31%) show very similar responses.

5.2 Effects of the CNT Volume Fraction

A study of the effects of CNT volume fraction is performed for a fixed volume fraction of fiber. CNT volume fraction ν_{CNT} reads as follows:

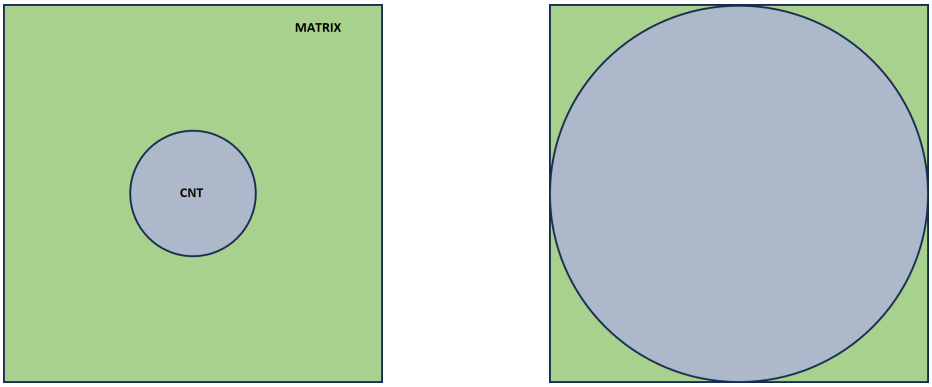
$$\nu_{CNT} = \frac{\pi r_{CNT}^2 l_{CNT} NO_{CNT}}{V_{RVE}}, \tag{5.2}$$

where r_{CNT}, l_{CNT}, NO_{CNT}, and V_{RVE} are the radius, length, and number of the CNT and volume of the RVE, respectively.

Table 5.5: The fixed parameters in the effects of the CNT volume fraction study with the fiber radius of 5 micrometers.

Parameter	**Value**
Fiber volume fraction ν_f	20% [-]
CNT radius r_{CNT}	7.1 [$\mathrm{n}m$]
CNT length l_{CNT}	2 [μm]

The critical parameters used in the studies are given in Table 5.5. When considering the radius of the CNT used in the models, there is an upper limit on the CNT volume fraction. As stated earlier in Chapter 4, CNTs' radius is assumed to be constant. With this assumption, the maximum volume fraction of the local CNT volume fraction becomes 78.54%, which results in a maximum CNT volume fraction of between 11 and 12, depending on the fiber volume fractions, i.e., fiber radius. The ratio of 78.54% comes from the case when the CTN touches the boundary of the RVE, as illustrated in Figure 5.5. Over this value, CNTs grown on the fiber surface intersect with each other, which is a nonphysical situation.



(a) (b)

Figure 5.5: Illustrations of 2D RVE consisting of single CNT and a matrix. (a) A CNT volume fraction is less than the maximum value. (b) The maximum volume fraction of CNT where the CNT touches the boundary of the RVE.

Table 5.6: CNT numbers corresponding to CNT volume fraction in the study of the effect of the CNT volume fraction for the varying CNT number case.

CNT Volume Fraction	0.1	0.5	1.5	3
Number of CNTs	0.1×10^7	0.6×10^7	1.8×10^7	3.7×10^7
CNT Volume Fraction	5	7	9.4	11
Number of CNTs	6.3×10^7	8.8×10^7	11.9×10^7	13.8×10^7

Table 5.7: CNT lengths corresponding to CNT volume fraction in the study of the effect of the CNT volume fraction for the varying CNT length case.

CNT Volume Fraction	0.62	1.25	3
Length of CNTs	$0.2\mu m$	$0.5\mu m$	$1.2\mu m$
CNT Volume Fraction	4	7	11
Length of CNTs	$1.6\mu m$	$2.8\mu m$	$4.4\mu m$

In order to change the volume fraction of the CNT, the CNT length or number can be changed. Two parametric studies are carried out to observe the effects of the CNT

volume fraction. In the first study, the number of CNTs is changed to increase the CNT volume fraction while the CNT length is kept constant. In the second study, the CNT length is increased to increase the CNT volume fraction, where the CNT number is kept constant. The number and the length of CNTs corresponding to the CNT volume fraction are given in Table 5.6 and Table 5.7. As the CNT volume changes, the matrix volume fraction changes, respectively. The effects of the CNT volume fraction in both studies on engineering constants are presented in Figure 5.6.

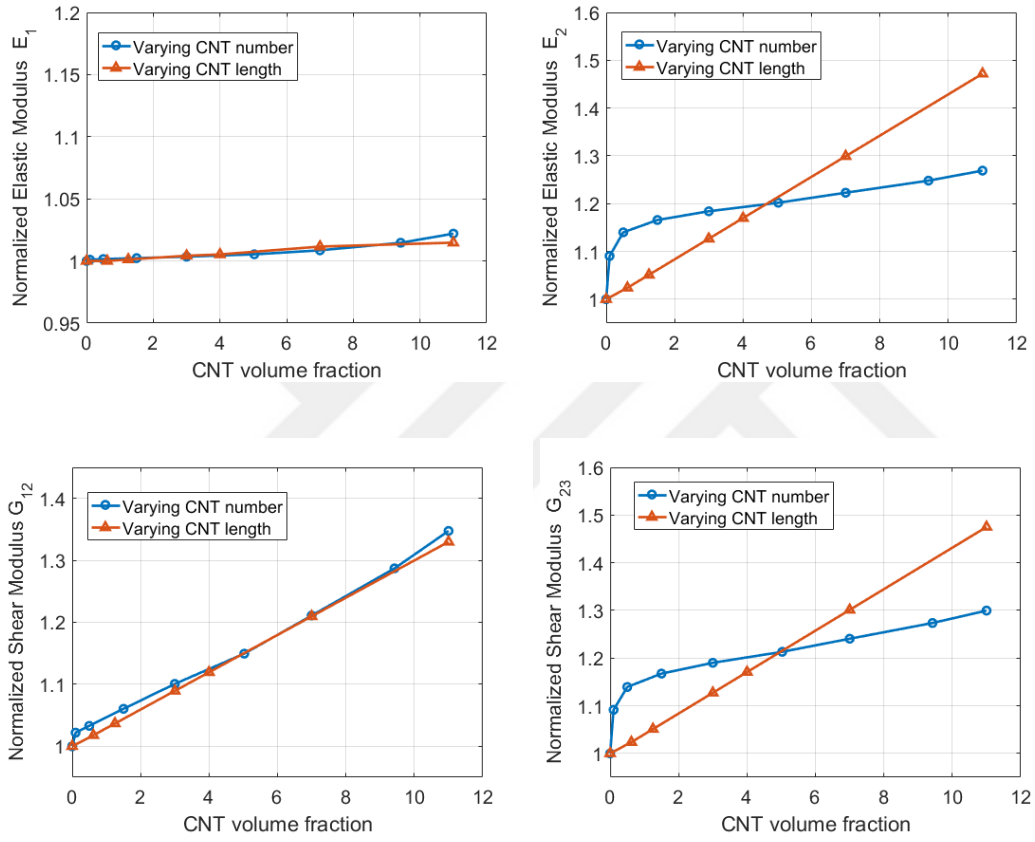


Figure 5.6: : Effects of the CNT volume fraction on engineering constants. The length of the CNTs is 2 micrometers for the varying CNT number case.

Based on the results, increasing the volume fraction of the CNT enhances the transverse elastic modulus and shear modulus perpendicular to the fiber direction by up to 50% and shear modulus parallel to the fiber direction by up to 35%. However, elastic modulus in the fiber direction is not affected by grafting CNT on the fiber. It can be

concluded from the results that increasing the volume fraction of CNT stiffens the interphase, which reveals that the effective engineering constants of the FFC increase with the CNT volume fraction.

Increasing the CNT volume fraction by either increasing the CNT length or increasing the CNT number does not affect the elastic modulus in the fiber direction E_1. For the constant CNT length study, the sudden increase in the other engineering constants from the no-CNT case originated from the sudden introduction of a thick interphase (2 micrometers). A constant CNT length also means a constant interphase thickness.

The shear modulus parallel to the fiber direction G_{12} has a similar trend for both studies. The elastic modulus in the transverse direction E_2 and the shear modulus perpendicular to the fiber direction G_{23} have different trends when the constant CNT length and constant CNT number approaches are compared. For the lower CNT volume fractions ($\nu_{CNT} < 5\%$), the constant CNT length approach overestimates the effective engineering constants E_2 and G_{23}, where the constant CNT number overestimates when the CNT volume fraction is higher ($\nu_{CNT} > 5\%$). The results of E_2 and G_{23} are the same at the CNT volume fraction of 5% because the CNT length becomes the same (2 micrometers) in both models.

5.3 Effects of the CNT Length

CNT length's effects on engineering constants are studied for a fixed fiber, CNT, and matrix volume fraction. Only the length of the CNTs is changed. The CNT volume fraction is written in Equation 5.2. In order to keep the CNT volume fraction constant, as the length of CNTs increases, the number of the CNTS is decreased respectively. All other parameters in Equation 5.2 are kept constant.

Table 5.8: The parameters in the effects of the CNT length study with the constant CNT volume fraction.

Parameter	Value
Fiber volume fraction ν_f	20% [-]
CNT radius r_{CNT}	7.1 [$\mathrm{n}m$]
CNT length l_{CNT}	2, 3, 4 [μm]

The critical parameters used in the studies are given in Table 5.9. The effects of CNT length on engineering constants are presented in Figure 5.7.

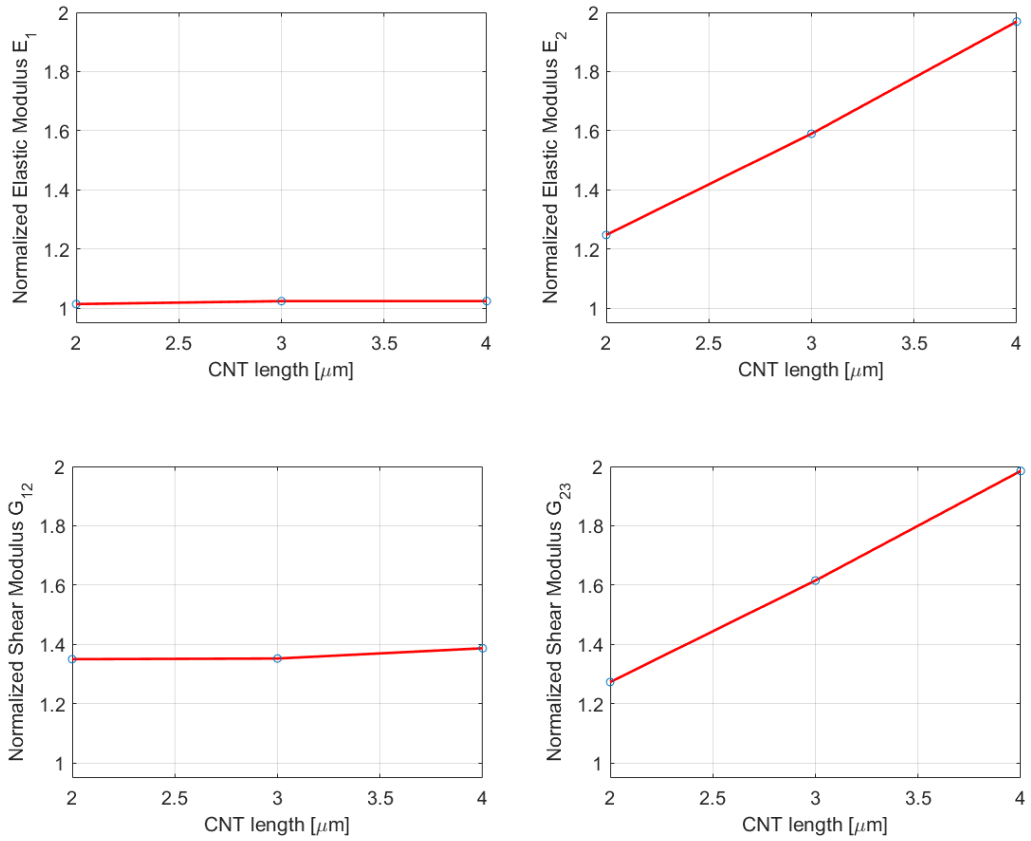


Figure 5.7: Effects of the CNT length on engineering constants. The CNT volume fraction is constant and 9.42% in the study. The fiber radius is 5 micrometers, and the fiber volume fraction is 20%.

Increasing the length of CNT while keeping the total volume fraction the same thickens and softens the interphase at the same time. It can be concluded from the results that doubling the CNT length increases the transverse elastic modulus E_2 and shear modulus G_{23} by about 60%, while the tensile elastic modulus E_1 and shear modulus G_{12} change by less than 2%.

5.4 Effects of the Fiber Volume Fraction

Finally, the effects of fiber volume fraction are studied for a fixed CNT volume fraction. The number, length, and radius of the CNTs are kept constant. The RVE of the study is constructed with a single carbon fiber, as seen in Figure 4.4. Multiple fibers in RVE could not have been used because of the complexity of the model and the size differences between the CNT and carbon fiber, as explained in Chapter 4. With the multiple fiber RVE, the degrees of freedom in the FE model increase drastically, which makes the solution computationally unaffordable. Hence, the fiber volume fraction is increased by increasing the fiber radius.

Table 5.9: The parameters in the effects of the fiber volume fraction study with the constant CNT volume fraction.

Parameter	**Value**
Fiber volume fraction ν_f	12.5-28% [-]
CNT radius r_{CNT}	7.1 [$\mathrm{n}m$]
CNT length l_{CNT}	3 [μm]

The critical parameters used in the studies are given in Table 5.9. In this study, normalized engineering constants are calculated with respect to the no CNT-grown cases of each fiber volume fraction case. Normalized engineering constants can be rewritten as

$$\beta_{normalized} = \frac{\beta_{\nu_f}}{\beta_{\nu_f @ \nu_{CNT=0}}}, \tag{5.3}$$

where β_{ν_f} and $\beta_{\nu_f @ \nu_{CNT=0}}$ are any property where the CNT volume fraction is any value other than zero and any property where the CNT volume fraction equals to zero for the same volume fraction of fiber.

The effects of fiber volume fraction on engineering constants are presented in Figure 5.8.

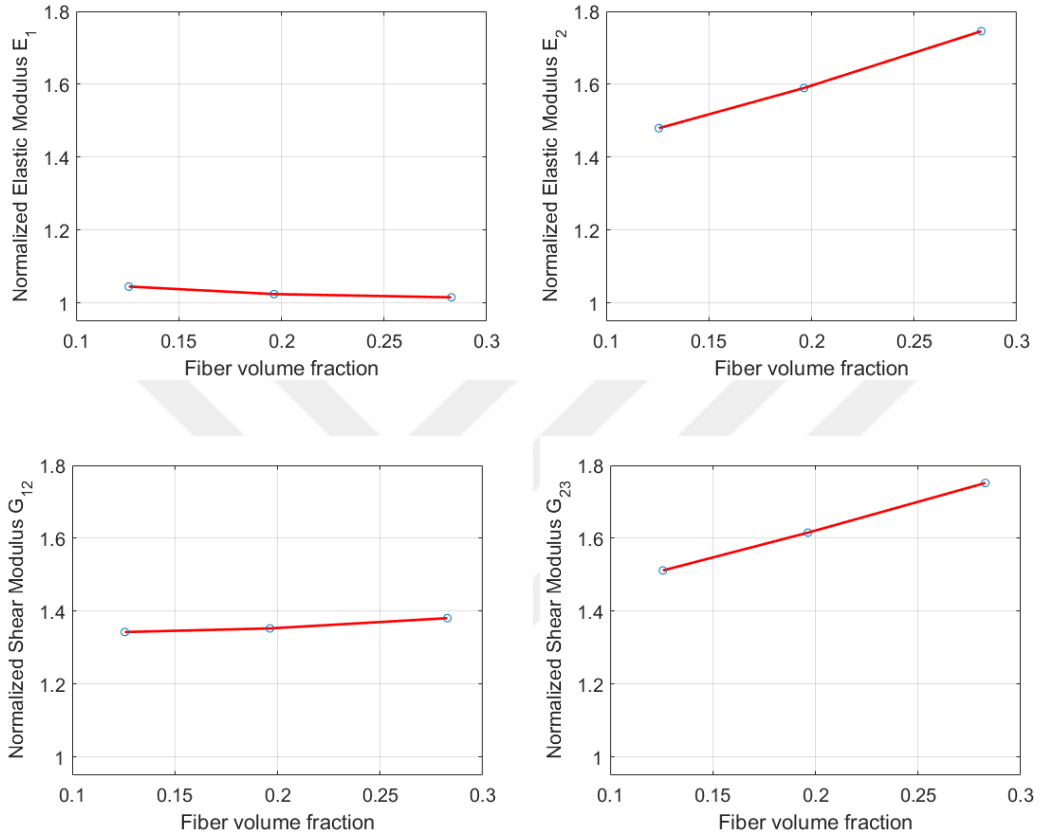


Figure 5.8: Effects of the fiber volume fraction on engineering constants. The CNT volume fraction is constant and 9.42% in the study; the length (2 micrometers) and the number (8×10^6) of CNTs are fixed, which results in different local CNT volume fractions in the interphase regions.

It can be concluded from the results that grafting CNTs with the same volume fraction, length, and number on different volume fractions of fiber has different effects. For higher fiber volume fractions of FFCs, increments in the elastic modulus E_2 and the shear modulus G_{23} are increased by up to 75% for the fiber volume fraction of 28%. The elastic modulus E_1 and the shear modulus G_{12} can be considered un-

affected by the fiber volume fraction. E_1 is slightly decreased and G_{23} is slightly increased compared to fiber volume fraction of 12.5%.

CHAPTER 6

CONCLUSION

In this thesis, the structure, manufacturing, characterization, and enhanced properties of FFCs are presented. The mechanical enhancements of grafting CNTs on the fiber's surface are discussed. The two challenging areas of advanced composites, manufacturing and characterization, are concerned, and studies from the literature are explained. The homogenization method, which is to characterize hybrid composites in the scope of the thesis, is explained. Voigt-Reuss, Hashin-Shtrikman, Mori-Tanaka, and computational homogenization methods are discussed and compared. The procedure for calculating the homogenized engineering constants is explained for a transversely isotropic material. The graded structure of the interphase is discussed in the thesis. The local CNT volume fraction in the interphase region decreases as the distance from the fiber surface increases. Due to the graded structure of the interphase and the size difference of the constituents, which is in the order of thousands, homogenizing the FFC in a single model becomes computationally expensive. Therefore, a two-step computational homogenization approach is proposed, and the details of the approach are explained. A schematic procedure of the two-step computational homogenization approach is given in Figure 4.7.

The application of the boundary conditions for the homogenization of FFC is discussed in the thesis. Periodic boundary conditions (PBC) are the most commonly applied conditions for periodic RVEs. However, applying the PBCs for the homogenization of the FFC is challenging because of the complexity and the mesh density of the RVE. Therefore, linear displacement boundary conditions (DBC) are employed. In order to get converged results for the FFC, the size of the RVE is studied. It is

concluded from the results that the shear modulus parallel to the fiber direction and the transverse elastic modulus are the most affected constants. In order to compute converged values of these constants, a long square prism with an aspect ratio of 50 is chosen as the RVE of the FFC.

The effective elastic properties of the FFC were studied using a two-step computational homogenization approach. The first step uses a micromechanics-based Mori-Tanaka method to homogenize functionally graded interphase. Using the Mori-Tanaka method gives very accurate results and is advantageous regarding computational cost. In the second step, an RVE is constructed for 3-phase fuzzy fiber and homogenized using FEM. The effective properties are compared with grafting CNTs on fiber with a base fiber-reinforced polymer composite. The effects of CNT volume fraction, length, and fiber volume fraction are studied.

The following conclusions can be drawn:

- Homogenizing the hybrid composites with the computational homogenization approach can be costly due to the functionally graded interphase and the scale difference of the constituents. However, the proposed two-step homogenization approach provides a cost-effective solution.
- Grafting CNTs on the fiber surface, in general, increases the effective properties of the composite material, which increases the fiber's surface area, providing more effective load transfer between the fiber and the matrix.
- The results reveal that the FFCs have enhancements in engineering constants of transverse elastic modulus and shear modulus parallel and perpendicular to the fiber direction. However, grafting the CNTs on the fiber surface does not affect the elastic modulus in the fiber direction.
- Parametric study of the CNT volume fraction shows that increasing the volume fraction of the CNT enhances the engineering constants of the FFC where the change in the fiber direction elastic modulus is negligible.
- Increasing the length of the CNTs while keeping the volume fraction of CNT constant increases the transverse elastic modulus and the shear modulus parallel

to the fiber direction of the FFC. The tensile elastic modulus and the shear modulus perpendicular to the fiber direction are not affected by the length of the CNTs.

- Grafting CNTs with the same volume fraction, length, and number on different volume fractions of fiber has different effects. For higher volume fractions of the carbon fiber, enhancements in the transverse shear modulus and the shear modulus parallel to the fiber direction are higher.

- It is observed from the results that increasing the CNT length compared to increasing the CNT volume fraction enhances the composites' effective properties more significantly.

The following points can be studied as future works:

- In this study, CNTs waviness is not considered. The effect of the CNT waviness can be included.
- In the literature, an interphase between the CNT and the matrix is studied. The effect of the interphase can be included.
- Because of the complexity and the mesh density of the RVE, periodic boundary conditions could not be applied. A further study can be conducted to construct a better RVE for applying periodic boundary conditions.
- Effects of grafting CNTs on piezoelectric fibers on piezoelectric constants are studied in the literature. This study can be extended to piezoelectric fiber-reinforced composites.
- The study is limited to linear elasticity. Failure modes and mechanics are studied in several experimental works in the literature. Failure mechanics of the FFC can be studied with a computational approach.

REFERENCES

[1] M. Kulkarni, D. Carnahan, K. Kulkarni, D. Qian, and J. L. Abot, "Elastic response of a carbon nanotube fiber reinforced polymeric composite: A numerical and experimental study," *Composites Part B: Engineering*, vol. 41, no. 5, pp. 414–421, 2010.

[2] H.-Z. Shan and T.-W. Chou, "Transverse elastic moduli of unidirectional fiber composites with fiber/matrix interfacial debonding," *Composites Science and Technology*, vol. 53, no. 4, pp. 383–391, 1995.

[3] D. Güzel, "A two-level homogenization method for polymer nancomposites with coated inclusions," Master's thesis, Middle East Technical University, 2019.

[4] A. Aqel, K. M. A. El-Nour, R. A. Ammar, and A. Al-Warthan, "Carbon nanotubes, science and technology part (i) structure, synthesis and characterisation," *Arabian Journal of Chemistry*, vol. 5, no. 1, pp. 1–23, 2012.

[5] Y. Zhang, Y. Bai, and B. Yan, "Functionalized carbon nanotubes for potential medicinal applications," *Drug discovery today*, vol. 15, pp. 428–35, 05 2010.

[6] R. Li, N. Lachman, P. Florin, H. D. Wagner, and B. L. Wardle, "Hierarchical carbon nanotube carbon fiber unidirectional composites with preserved tensile and interfacial properties," *Composites Science and Technology*, vol. 117, pp. 139–145, 2015.

[7] F. Shan, Y. Gu, M. Li, Y. Liu, and Z. Zhang, "Effect of deposited carbon nanotubes on interlaminar properties of carbon fiber-reinforced epoxy composites using a developed spraying processing," *Polymer Composites*, vol. 34, 01 2013.

[8] F. Larsson, K. Runesson, S. Saroukhani, and R. Vafadari, "Computational homogenization based on a weak format of micro-periodicity for rve-problems,"

Computer Methods in Applied Mechanics and Engineering, vol. 200, no. 1, pp. 11–26, 2011.

[9] Y. Cheng, K. Zhang, B. Liang, H. Cheng, G. Hou, G. Xu, and W. Jin, "Micromechanics of cnt grafted frp based on hierarchical homogenization of transversely isotropic multi-coated model," *International Journal of Mechanical Sciences*, vol. 161-162, p. 105014, 2019.

[10] B. Sabuncuoglu, L. Gorbatikh, and S. V. Lomov, "Analysis of stress concentrations in transversely loaded steel-fiber composites with nano-reinforced interphases," *International Journal of Solids and Structures*, vol. 130-131, pp. 248–257, 2018.

[11] D. Güzel and E. Gürses, "A two-level homogenization approach for polymer nanocomposites with coated inclusions," *Procedia Structural Integrity*, vol. 35, pp. 34–41, 2022.

[12] H. Kim, E. Oh, H. T. Hahn, and K.-H. Lee, "Enhancement of fracture toughness of hierarchical carbon fiber composites via improved adhesion between carbon nanotubes and carbon fibers," *Composites Part A: Applied Science and Manufacturing*, vol. 71, pp. 72–83, 2015.

[13] N. Karim, M. A. Patwary, S. Abedin, R. Hossen, and M. Rahman, "A review on carbon nanotubes: Preparation, properties and applications," *Journal of Research Updates in Polymer Science*, vol. 9, 01 2022.

[14] G. Chatzigeorgiou, Y. Efendiev, and D. C. Lagoudas, "Homogenization of aligned "fuzzy fiber" composites," *International Journal of Solids and Structures*, vol. 48, no. 19, pp. 2668–2680, 2011.

[15] S. S. Wicks, R. G. de Villoria, and B. L. Wardle, "Interlaminar and intralaminar reinforcement of composite laminates with aligned carbon nanotubes," *Composites Science and Technology*, vol. 70, no. 1, pp. 20–28, 2010.

[16] E. J. Garcia, B. L. Wardle, A. John Hart, and N. Yamamoto, "Fabrication and multifunctional properties of a hybrid laminate with aligned carbon nanotubes grown in situ," *Composites Science and Technology*, vol. 68, no. 9, pp. 2034–2041, 2008.

[17] C. D. Wood, M. J. Palmeri, K. W. Putz, G. Ho, R. Barto, and L. Catherine Brinson, "Nanoscale structure and local mechanical properties of fiber-reinforced composites containing mwcnt-grafted hybrid glass fibers," *Composites Science and Technology*, vol. 72, no. 14, pp. 1705–1710, 2012.

[18] S. Dhala and M. Ray, "Micromechanics of piezoelectric fuzzy fiber-reinforced composite," *Mechanics of Materials*, vol. 81, pp. 1–17, 2015.

[19] H. De Luca, D. Anthony, E. Greenhalgh, A. Bismarck, and M. Shaffer, "Piezoresistive structural composites reinforced by carbon nanotube-grafted quartz fibres," *Composites Science and Technology*, vol. 198, p. 108275, 2020.

[20] K. zhi Li, L. Li, H. jun Li, Q. Song, J. hua Lu, and Q. gang Fu, "Electrophoretic deposition of carbon nanotubes onto carbon fiber felt for production of carbon/-carbon composites with improved mechanical and thermal properties," *Vacuum*, vol. 104, pp. 105–110, 2014.

[21] R. Hill, "Elastic properties of reinforced solids: Some theoretical principles," *Journal of the Mechanics and Physics of Solids*, vol. 11, no. 5, pp. 357–372, 1963.

[22] W. Voigt, *Lehrbuch der Kristallphysik (mit Ausschluss der Kristalloptik)*. Vieweg+Teubner Verlag, 1928.

[23] A. Reuss, "Berechnung der fließgrenze von mischkristallen auf grund der plastizitätsbedingung für einkristalle .," *ZAMM - Journal of Applied Mathematics and Mechanics / Zeitschrift für Angewandte Mathematik und Mechanik*, vol. 9, no. 1, pp. 49–58, 1929.

[24] Z. Hashin and S. Shtrikman, "A variational approach to the theory of the elastic behaviour of multiphase materials," *Journal of the Mechanics and Physics of Solids*, vol. 11, no. 2, pp. 127–140, 1963.

[25] J. D. Eshelby and R. E. Peierls, "The determination of the elastic field of an ellipsoidal inclusion, and related problems," *Proceedings of the Royal Society of London. Series A. Mathematical and Physical Sciences*, vol. 241, no. 1226, pp. 376–396, 1957.

[26] T. Mori and K. Tanaka, "Average stress in matrix and average elastic energy of materials with misfitting inclusions," *Acta Metallurgica*, vol. 21, no. 5, pp. 571–574, 1973.

[27] S. Hazanov, "Hill condition and overall properties of composites," *Archive of Applied Mechanics*, vol. 68, pp. 385–394, 1998.

[28] A. Denisiewicz, M. Kuczma, K. Kula, and T. Socha, "Influence of boundary conditions on numerical homogenization of high performance concrete," *Materials*, vol. 14, p. 1009, 02 2021.

[29] V.-D. Nguyen, E. Béchet, C. Geuzaine, and L. Noels, "Imposing periodic boundary condition on arbitrary meshes by polynomial interpolation," *Computational Materials Science*, vol. 55, pp. 390–406, 2012.

[30] A. Denisiewicz, M. Kuczma, K. Kula, and T. Socha, "Influence of boundary conditions on numerical homogenization of high performance concrete," *Materials*, vol. 14, p. 1009, 02 2021.

[31] X. Li, Y. Liang, Y. Du, K. Wan, and Q. Duan, "Computational multiscale methods for granular materials," *Theoretical and Applied Mechanics Letters*, vol. 3, no. 1, p. 011001, 2013.

[32] J.-L. Tsai, S.-H. Tzeng, and Y.-T. Chiu, "Characterizing elastic properties of carbon nanotubes/polyimide nanocomposites using multi-scale simulation," *Composites Part B: Engineering*, vol. 41, no. 1, pp. 106–115, 2010.

[33] S. Kundalwal and M. Ray, "Effective properties of a novel composite reinforced with short carbon fibers and radially aligned carbon nanotubes," *Mechanics of Materials*, vol. 53, pp. 47–60, 2012.

[34] M. Moakher, "Fourth-order cartesian tensors: old and new facts, notions and applications," *The Quarterly Journal of Mechanics and Applied Mathematics*, vol. 61, pp. 181–203, 01 2008.

[35] V. A. Lubarda and M. Chen, "On the elastic moduli and compliances of transversely isotropic and orthotropic materials," *Journal of Mechanics of Materials and Structures*, vol. 3, pp. 153–171, 2008.

[36] Y. Qiu and G. Weng, "On the application of mori-tanaka's theory involving transversely isotropic spheroidal inclusions," *International Journal of Engineering Science*, vol. 28, no. 11, pp. 1121–1137, 1990.

[37] D. S. Simulia, "Abaqus 6.12 analysis user's manual providence," *RI, USA*, 2012.

[38] S. Kundalwal and M. Ray, "Effective properties of a novel continuous fuzzy-fiber reinforced composite using the method of cells and the finite element method," *European Journal of Mechanics - A/Solids*, vol. 36, pp. 191–203, 2012.

[39] L. J. Walpole, "Fourth-rank tensors of the thirty-two crystal classes: Multiplication tables," *Proceedings of the Royal Society of London. Series A, Mathematical and Physical Sciences*, vol. 391, no. 1800, pp. 149–179, 1984.

[40] R. M. Brannon, "Voigt and mandel components," in *Rotation, Reflection, and Frame Changes*, 2053-2563, pp. 26–1 to 26–20, IOP Publishing, 2018.

[41] S. Jacques, I. De Baere, and W. Van Paepegem, "Application of periodic boundary conditions on multiple part finite element meshes for the meso-scale homogenization of textile fabric composites," *Composites Science and Technology*, vol. 92, pp. 41–54, 2014.

Appendix A

A.1 Inverse of a Symmetric Fourth-Order Tensor

In this appendix, taking the inverse of a symmetric fourth-order tensor is explained. Let's define a fourth-order tensor $\mathbf{A}$

$$\mathbf{A} = A_{ijkl} = e_i \otimes e_j \otimes e_k \otimes e_l. \tag{A.1}$$

The inverse of the tensor of $\mathbf{A}$ is denoted as

$$\mathbf{A}^{-1} : \mathbf{A} = \mathbf{A} : \mathbf{A}^{-1} = \mathbf{I}, \tag{A.2}$$

where $\mathbf{I}$ is the fourth order identity tensor. If the tensor $\mathbf{A}$ is symmetric, the inverse of the tensor is also symmetric.

Walpole [39] states that a fourth-order can be expressed as

$$\mathbf{D}(\mathbf{A}) = \begin{bmatrix} A_{1111} & A_{1122} & A_{1133} & \sqrt{2}A_{1123} & \sqrt{2}A_{1113} & \sqrt{2}A_{1112} \\ A_{2211} & A_{2222} & A_{2233} & \sqrt{2}A_{2223} & \sqrt{2}A_{2213} & \sqrt{2}A_{2212} \\ A_{3311} & A_{3322} & A_{3333} & \sqrt{2}A_{3323} & \sqrt{2}A_{3313} & \sqrt{2}A_{3312} \\ \sqrt{2}A_{2311} & \sqrt{2}A_{2322} & \sqrt{2}A_{2333} & 2A_{2323} & 2A_{2313} & 2A_{2312} \\ \sqrt{2}A_{1311} & \sqrt{2}A_{1322} & \sqrt{2}A_{1333} & 2A_{1323} & 2A_{1313} & 2A_{1312} \\ \sqrt{2}A_{1211} & \sqrt{2}A_{1222} & \sqrt{2}A_{1233} & 2A_{1223} & 2A_{1213} & 2A_{1212} \end{bmatrix}. \tag{A.3}$$

When the tensor is symmetric, the above-expressed notation, also known as the Mandel representation [40], reads as

$$\mathbf{D}(\mathbf{A} : \mathbf{A^{-1}}) = \mathbf{D}(\mathbf{A}) \cdot \mathbf{D}(\mathbf{A^{-1}}). \tag{A.4}$$

Then, the inverse of a symmetric fourth-order tensor in Mandel reads as

$$\mathbf{D}(\mathbf{A^{-1}}) = \mathbf{D}(\mathbf{A})^{-\mathbf{1}} \tag{A.5}$$

The inverse of a symmetric fourth-order tensor can be calculated using the Mandel representation. The symmetric fourth-order tensor is mapped into a six-by-six matrix (Mandel form), and then the inverse to the Mandel form is taken using simple calculus. The inverse Mandel form is mapped back to the fourth-order tensor form using the above representation.

Appendix B

B.1 Comparative Study of Periodic Boundary Conditions and Linear Displacement Boundary Conditions

In this Appendix, a comparative study of the application of periodic boundary conditions and displacement boundary conditions is discussed. As explained before in the thesis, periodic boundary conditions could not be applied because of the complexity and mesh density of the RVE. In order to apply the periodic boundary conditions, a simple model is preferred. The RVE consists of 2 constituents, and the fiber is a square prism, as shown in Figure B.1.

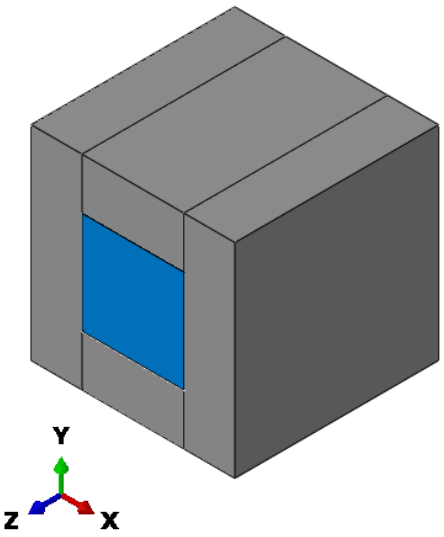


Figure B.1: The RVE of the simple model consists of 2 constituents, and the fiber is a square prism.

The periodic boundary conditions are applied, as explained in Chapter 3. For the comparison study, PBCs are applied on the cubic RVE shown in Figure B.1. Displacement boundary conditions are applied to three different RVEs having different aspect ratios. Illustrations of applications of the PBCs and DBCs are shown in Figure B.2.

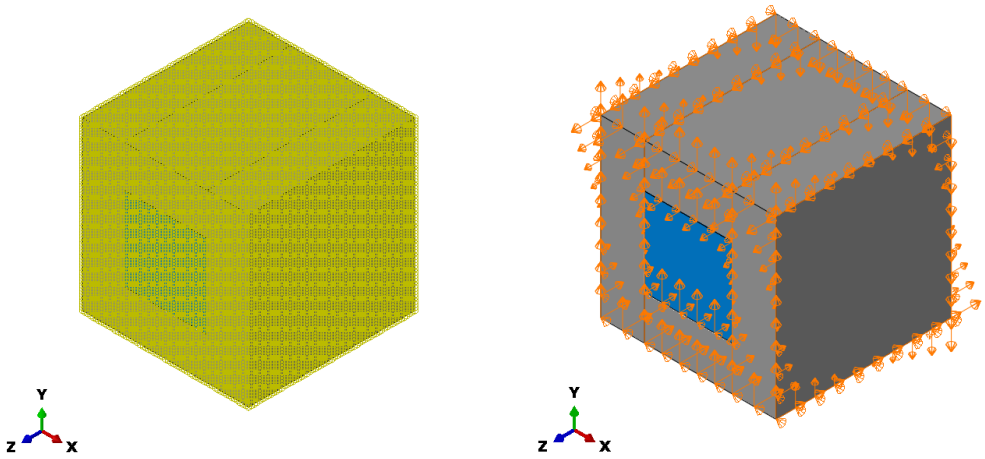


Figure B.2: Illustrations of applications of (a) PBCs and (b) DBCs.

Table B.1: Comparison of DBC and PBC results for different aspect ratios of the RVE.

	C_{11} [GPa]	C_{12} [GPa]	C_{22} [GPa]	C_{23} [GPa]	C_{55} [GPa]
DBC (AR=1)	61.22345	2.488047	5.993445	2.410294	5.124968
DBC (AR=8)	61.11404	2.297730	5.525619	2.216024	2.342126
DBC (AR=16)	61.10636	2.284366	5.492950	2.202200	2.133671
DBC (AR=33)	61.10252	2.277683	5.476613	2.195287	2.029441
DBC (AR=50)	61.10159	2.276061	5.471235	2.191285	1.997217
PBC (AR=1)	61.26003	2.263430	5.430770	2.184161	1.889445

Four RVEs are constructed with different aspect ratios of 1, 8, 16, and 33 for applying DBCs. PBCs are applied to the cubic RVE having an aspect ratio of 1. The results of

the study are presented in Table B.1, and convergence trends are shown in Figure B.3.

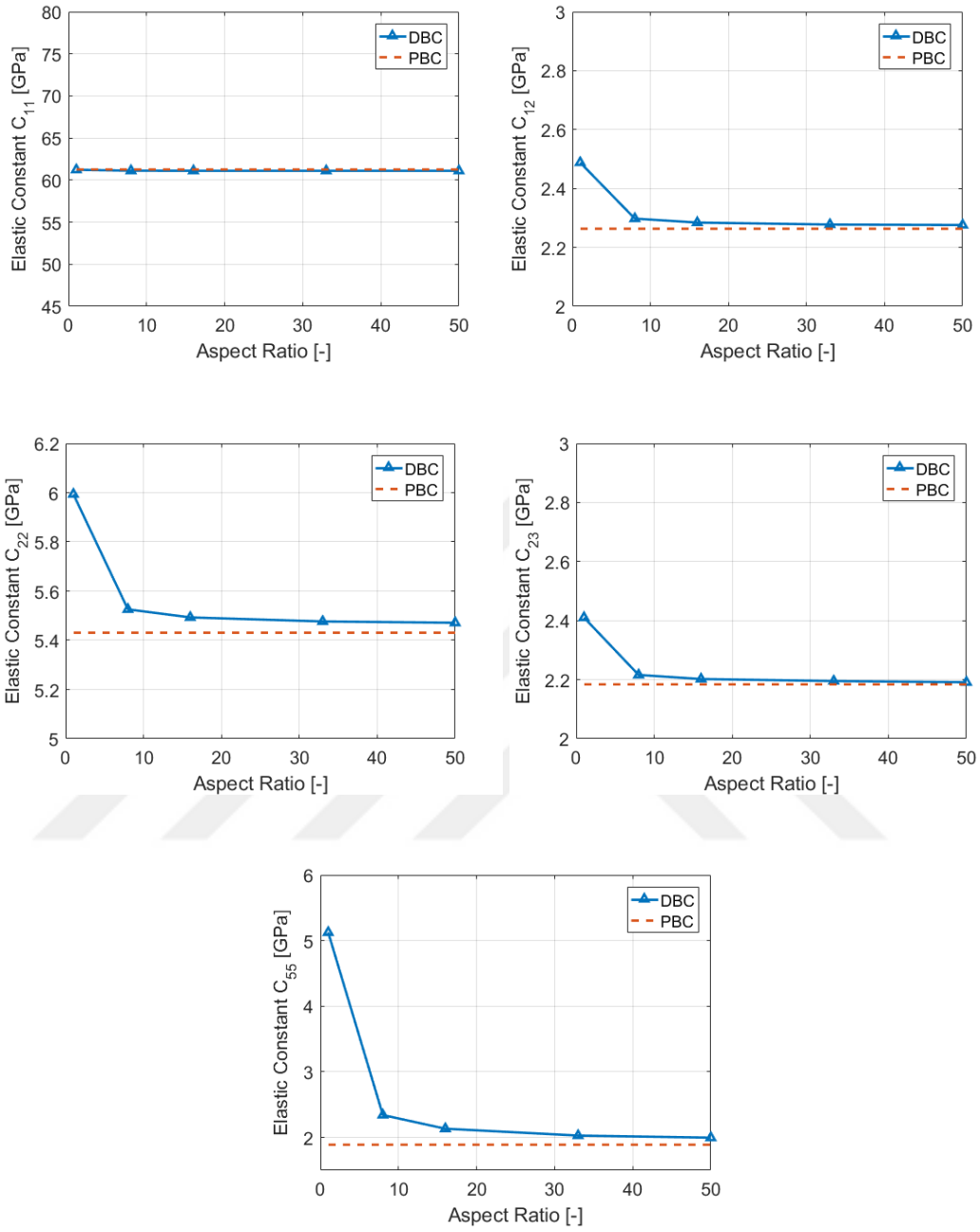


Figure B.3: Comparison of DBC and PBC results for different aspect ratios of the RVE.

The results show that the most affected elastic constant is C_{55}, the shear modulus parallel to the fiber direction. The literature studies stated that PBCs give the most

accurate results for the shear modulus of the periodic structures [41]. The comparative study presented here reveals the same result. After increasing the aspect ratio of the RVE, results do not change much, and the aspect ratio of 50 difference in the C_{55} constant is less than 2%. Based on the results, the aspect ratio of the RVE of the FFC is decided to be 50 in this thesis, and the results are obtained by applying DBCs to the RVE having the aspect ratio of 50.

Appendix C

C.1 FORTRAN Script for the Homogenization of Interphase

In this appendix, the FORTRAN script used in the ABAQUS USDFL subroutine for the homogenization of the interphase is given.

Listing C.1: Fortran script for the ABAQUS USDFL subroutine

```
      SUBROUTINE USDFLD(FIELD,STATEV,PNEWDT,
     1 DIRECT,T,CELENT,TIME,DTIME,CMNAME,ORNAME,
     2 NFIELD,NSTATV,NOEL,NPT,LAYER,KSPT,KSTEP,
     3 KINC,NDI,NSHR,COORD,JMAC,JMATYP,MATLAYO,
     4 LACCFLA)
C
      INCLUDE 'ABAPARAM.INC'
C
      CHARACTER*80 CMNAME,ORNAME
      CHARACTER*3 FLGRAY(15)
      DIMENSION FIELD(NFIELD),STATEV(NSTATV),
     1 DIRECT(3,3),T(3,3),TIME(2)
      DIMENSION ARRAY(15),JARRAY(15),JMAC(*),
     2 JMATYP(*),COORD(*)
      X=COORD(1)
        Y=COORD(2)
        FIELD(1)=SQRT(X*X+Y*Y)
      RETURN
```

```
END
```

Appendix D

D.1 MATLAB Script for the Homogenization of FFC

In this appendix, the MATLAB script for the homogenization of the FFC is given.

Listing D.1: Matlab script for the homogenization of FFC

```
   Import data from text file.
  Script for importing data from the following text file:

     C: Users o5533 OneDrive   metu.edu.tr Desktop Abaqus11 1 1
    LOAD abaqus.rpt

clc;clear all;
   Initialize variables.
 ONLY CHANGE HERE TO RUN NEW HOMOGENIZATION
filename =  C: Temp DBCSQlonggg13.rpt ;
startRow = 14;
RESOUT= DBCSQlonggg13.txt ;
   Read columns of data as strings:
  For more information, see the TEXTSCAN documentation.
formatSpec =  16s 16s 16s 16s 16s 16s 16s 16s 16s 16s 16s 16s
    16s s [  n r] ;

   Open the text file.
fileID = fopen(filename, r ) ;
```

```
   Read columns of data according to format string.
  This call is based on the structure of the file used to generate
    this
  code. If an error occurs for a different file, try regenerating
   the code
  from the Import Tool.
textscan(fileID,   [  n r] , startRow 1 ,  WhiteSpace ,   ,
   ReturnOnError , false);
dataArray = textscan(fileID, formatSpec,  Delimiter ,   ,
   WhiteSpace ,   ,  ReturnOnError , false);

   Close the text file.
fclose(fileID);

   Convert the contents of columns containing numeric strings to
   numbers.
  Replace non numeric strings with NaN.
raw = repmat (   , length(dataArray 1 ) ,length(dataArray) 1);
for col=1:length(dataArray) 1
    raw(1:length(dataArray col ) ,col) = dataArray col ;
end
numericData = NaN(size(dataArray 1 , 1 ) ,size(dataArray,2));

for col=[1,2,3,4,5,6,7,8,9,10,11,12,13,14,15]
      Converts strings in the input cell array to numbers.
       Replaced non numeric
      strings with NaN.
    rawData = dataArray col ;
    for row=1:size(rawData, 1);
          Create a regular expression to detect and remove non
           numeric prefixes and
```

```
            suffixes.
        regexstr =  (?prefix .?)(?numbers ([ ] (d+[ ,])
            +[ .]0 ,1 d [eEdD]0 ,1 [ +] d [i]0 ,1) ([ ] (d
            +[ ,]) [ .] 1 ,1 d+[eEdD]0 ,1 [ +] d [i]0 ,1))(?
            suffix . ) ;
        try
            result = regexp(rawData row ,  regexstr,  names );
            numbers = result.numbers;

              Detected commas in non thousand locations.
            invalidThousandsSeparator = false;
            if any(numbers== , );
                thousandsRegExp =    d+?( ,d 3 )  . 0 ,1 d   ;
                if isempty(regexp(numbers, thousandsRegExp,  once
                    ));
                    numbers = NaN;
                    invalidThousandsSeparator = true;
                end
            end
              Convert numeric strings to numbers.
            if  invalidThousandsSeparator;
                numbers = textscan(strrep(numbers,  , ,   ),   f )
                    ;
                numericData(row, col) = numbers 1 ;
                raw row, col  = numbers 1 ;
            end
        catch me
        end
    end
end
```

```
   Replace non numeric cells with NaN
R = cellfun(@(x)  isnumeric(x)     islogical(x),raw);   Find non
   numeric cells
raw(R) =  NaN ;   Replace non numeric cells

   Allocate imported array to column variable names
Elementnum= cell2mat(raw(:, 1));
 Intpt = cell2mat(raw(:, 2));
E11 = cell2mat(raw(:, 3));
E22 = cell2mat(raw(:, 4));
E33 = cell2mat(raw(:, 5));
E12 = cell2mat(raw(:, 6));
E13 = cell2mat(raw(:, 7));
E23 = cell2mat(raw(:, 8));
S11 = cell2mat(raw(:, 9));
S22 = cell2mat(raw(:, 10));
S33 = cell2mat(raw(:, 11));
S12 = cell2mat(raw(:, 12));
S13 = cell2mat(raw(:, 13));
S23 = cell2mat(raw(:, 14));
IVOL = cell2mat(raw(:, 15));


   Clear temporary variables
clearvars filename startRow formatSpec fileID dataArray ans raw
   col numericData rawData row regexstr result numbers
   invalidThousandsSeparator thousandsRegExp me R;

   Homogenization procedure

HE11=0;HE22=0;HE33=0;HE12=0;HE13=0;HE23=0;
HS11=0;HS22=0;HS33=0;HS12=0;HS13=0;HS23=0;
```

```
SUMIVOL=0;

for i=1:length(IVOL)
    if isnan(Elementnum(i))
        continue;
    end
    HE11=HE11+E11(i) IVOL(i);
    HE22=HE22+E22(i) IVOL(i);
    HE33=HE33+E33(i) IVOL(i);
    HE12=HE12+E12(i) IVOL(i);
    HE13=HE13+E13(i) IVOL(i);
    HE23=HE23+E23(i) IVOL(i);
    HS11=HS11+S11(i) IVOL(i);
    HS22=HS22+S22(i) IVOL(i);
    HS33=HS33+S33(i) IVOL(i);
    HS12=HS12+S12(i) IVOL(i);
    HS13=HS13+S13(i) IVOL(i);
    HS23=HS23+S23(i) IVOL(i);
    SUMIVOL=SUMIVOL+IVOL(i);
end

homoE11=HE11/SUMIVOL;homoE22=HE22/SUMIVOL;homoE33=HE33/
   SUMIVOL;

homoE12=HE12/SUMIVOL;homoE13=HE13/SUMIVOL;homoE23=HE23/
   SUMIVOL;

homoS11=HS11/SUMIVOL;homoS22=HS22/SUMIVOL;homoS33=HS33/
   SUMIVOL;

homoS12=HS12/SUMIVOL;homoS13=HS13/SUMIVOL;homoS23=HS23/
   SUMIVOL;
```

```
   Calculation of elasticity tensor
  C11=homoS11/homoE11;
  C12=homoS22/homoE11;
  C13=homoS33/homoE11;
C21=homoS11/homoE22;
C22=homoS22/homoE22;
C23=homoS33/homoE22;
  C44=homoS23/homoE23;
  C31=homoS33/homoE11;
  C23=homoS22/homoE33;
C55=homoS13/homoE13;

     Write Results
text=fopen(RESOUT,w);
  format long
fprintf(text, sn, E11=  );fprintf(text, en,homoE11);
fprintf(text, sn, S11=  );fprintf(text, en,homoS11);
fprintf(text, sn, E22=  );fprintf(text, en,homoE22);
fprintf(text, sn, S22=  );fprintf(text, en,homoS22);
fprintf(text, sn, E33=  );fprintf(text, en,homoE33);
fprintf(text, sn, S33=  );fprintf(text, en,homoS33);
fprintf(text, sn, E12=  );fprintf(text, en,homoE12);
fprintf(text, sn, S12=  );fprintf(text, en,homoS12);
fprintf(text, sn, E13=  );fprintf(text, en,homoE13);
fprintf(text, sn, S13=  );fprintf(text, en,homoS13);
fprintf(text, sn, E23=  );fprintf(text, en,homoE23);
fprintf(text, sn, S23=  );fprintf(text, en,homoS23);
  fprintf(text, sn, C21=  );fprintf(text, en,C21);
  fprintf(text, sn, C22=  );fprintf(text, en,C22);
  fprintf(text, sn, C23=  );fprintf(text, en,C23);
  fprintf(text, sn, C11=  );fprintf(text, en,C11);
```

```
  fprintf(text , " s n , " C 12=  " );fprintf(text , " e n , " C 12);
  fprintf(text , " s n , " C 13=  " );fprintf(text , " e n , " C 13);
fprintf(text , " s n , " C 55=  " );fprintf(text , " e n , " C 55);
text=fclose( all );
```